Metal-Metal Multiple Bonds. 20.[1] Structural, Kinetic, and Theoretical Studies of the Reactivity of Dimolybdenum μ-Alkylidenes toward Small Molecules. Structures of $M_2(\mu\text{-}CAr_2)$, $M_2(\mu\text{-}CAr_2')$, and $M_2(\mu\text{-}\eta^1,\eta^2\text{-}i\text{-}PrNC{=}CAr_2')$ (M = Cp(or Cp')Mo(CO)$_2$, Ar = *p*-Tolyl, Ar_2' = 2,2'-Biphenylenyl, and Cp' = C_5H_4Me)

M. David Curtis,* L. Messerle, John J. D'Errico, Hugo E. Solis, Icela D. Barcelo, and W. M. Butler

Contribution from the Department of Chemistry, The University of Michigan, Ann Arbor, Michigan 48109. *Received November 12, 1986*

Abstract: The reactions of the dimolybdenum μ-alkylidene complexes $M_2(\mu\text{-}CAr_2)$ (M = Mo(CO)$_2$Cp or Cp' (Cp' = C_5H_4Me); Ar_2 = phenyl, *p*-tolyl (**2a,b**), or 2,2'-biphenylenyl (**2c**)) with CO, H_2, Ar_2CN_2, R_3P, isonitriles, alkenes, and alkynes are reported. The kinetics of the reaction of $M_2(\mu\text{-}CPh_2)$ with CO is interpreted in terms of the detachment of one coordinated phenyl group to provide a vacant coordination site prior to attack by CO. The differences in reactivity of **2a,b** compared with **2c** are explained on the basis of an EHMO analysis of the bonding in these complexes. The structures of **2b**, **2c**, and the reaction product $M_2(\mu\text{-}\eta^1,\eta^2\text{-}i\text{-}PrNC{=}CAr_2)$ (**8**), from **2c** and *i*-PrNC, are discussed, as are the dynamical behavior of these molecules in solution. Crystallographic data for **2b**·PhMe: a = 18.481 (8) Å, b = 19.095 (5) Å, c = 10.065 (3) Å, α = 90.01 (2)°, β = 105.76 (3)°, γ = 117.01 (3)°, V = 3014 (2) Å^3, Z = 4, ρ_c = 1.55 g/mL, space group = $P\bar{1}$, R_1, R_2 = 0.057, 0.078 on 6085 reflections with $I > 3\sigma(I)$. Crystallographic data for **2c**: a = 11.716 (5) Å, b = 12.152 (6) Å, c = 17.488 (4) Å, β = 108.77 (3)°, V = 2358 (2) Å^3, Z = 4, ρ_c = 1.76 g/mL, space group $P2_1/c$, R_1, R_2 = 0.036, 0.056 on 3381 reflections with $I > 3\sigma(I)$. Crystallographic data for **8**: a = 8.486 (3) Å, b = 20.16 (1) Å, c = 16.75 (7) Å, β = 92.31 (7)°, V = 2863 (4) Å^3, Z = 4, ρ_c = 1.71 g/mL, space group = $P2_1/c$, R_1, R_2 = 0.045, 0.039 on 2297 reflections with $I > 3\sigma(I)$.

In recent years, dinuclear alkylidene complexes have been suggested to be the catalytically active species in a variety of important processes. These include olefin metathesis,[2,3] alkyne polymerization,[2b,3b,4] and the Fischer-Tropsch synthesis.[5-7] As a result, bridging alkylidene complexes have been the object of intensive research.

Synthetic routes to μ-alkylidene complexes have recently been reviewed.[8,9] Although μ-alkylidene complexes have been prepared from phosphorus ylides,[10,11] ketenes,[12] organolithium[13] and magnesium[14] reagents, and dihaloalkanes,[15-17] the three most general approaches appear to be conversion of bridging groups, e.g., vinylidene, etc.,[18] addition of metal complexes across the M=C bond of mononuclear alkylidenes,[19,20] and the reaction of

Table I. Selected Bond Distances and Angles for **2b**

bond	distance (Å)	bond	angle (deg)
Mo1-C2	1.965 (13)	C27-C22-C23	116.9 (10)
Mo1-C1	1.989 (13)	C22-CB-C15	113.1 (9)
Mo2-C4	1.934 (13)	C22-CB-Mo2	125.7 (7)
Mo2-C3	1.937 (12)	C22-CB-Mo1	76.3 (6)
Mo2-C1	2.497 (13)	C15-CB-Mo2	114.1 (7)
Mo1-C22	2.343 (11)	C15-CB-Mo1	135.3 (7)
Mo1-C27	2.584 (11)	Mo2-CB-Mo1	88.4 (4)
CB-C22	1.437 (14)	O1-C1-Mo1	154.5 (11)
CB-C15	1.498 (14)	O2-C2-Mo1	176.3 (11)
Mo1-CB	2.222 (10)	O3-C3-Mo2	176.2 (11)
Mo2-CB	2.206 (10)	O4-C4-Mo2	179.4 (13)
C1-O1	1.159 (14)	C2-Mo1-C1	78.5 (5)
C2-O2	1.149 (14)	C2-Mo1-CB	120.9 (4)
C3-O3	1.147 (14)	C1-Mo1-CB	98.4 (5)
C4-O4	1.139 (14)	CB-Mo1-Mo2	45.6 (2)
C15-C20	1.384 (15)	CB-Mo2-Mo1	46.0 (3)
C15-C16	1.418 (15)	C1-Mo1-Mo2	53.8 (4)
C16-C17	1.416 (16)	C2-Mo1-Mo2	98.6 (4)
C17-C18	1.375 (16)	C1-Mo2-Mo1	40.0 (3)
C18-C19	1.399 (16)	C4-Mo2-Mo1	105.6 (3)
C18-C21	1.545 (18)	C3-Mo2-Mo1	88.4 (4)
C19-C20	1.400 (16)	C3-Mo2-CB	116.3 (4)
C22-C27	1.438 (14)	CB-Mo2-C1	85.2 (4)
C22-C23	1.449 (14)	C4-Mo2-C3	77.8 (5)
C23-C24	1.362 (16)	C4-Mo2-CB	76.8 (4)
C24-C25	1.436 (16)	CB-C22-C27	120.4 (10)
C25-C26	1.371 (16)	CB-C22-C23	122.3 (10)
C25-C28	1.525 (17)		
C26-C27	1.430 (15)		
Mo1-Mo2	3.087 (2)		
C-C(Cp)	1.41 (3) av		
Mo-C(Cp)	2.35 (4) av		

(1) Part 19 (Review) Curtis, M. D. *Polyhedron* **1987**, in press.
(2) (a) Garnier, F.; Krausz, P.; DuBois, J. *J. Organomet. Chem.* **1979**, *170*, 195. (b) Garnier, F.; Krausz, P. *J. Mol. Catal.* **1980**, *8*, 91.
(3) (a) Parker, A.; Rose, F.; Rudler, M.; Rudler, H. *J. Organomet. Chem.* **1982**, *235*, C13. (b) Rudler, H.; Rose, F.; Rudler, M.; Alvarez, C. *J. Mol. Catal.* **1982**, *15*, 81. (c) Levisalles, J.; Rose-Munch, F.; Rudler, H.; Daran, J.-C.; Jeannin, Y. *J. Chem. Soc., Chem. Commun.* **1981**, 1057. (d) Rudler, H. *J. Mol. Catal.* **1980**, *8*, 53.
(4) Levisalles, J.; Rose-Munch, F.; Rudler, H.; Daran, J.-C.; Dromzee, Y.; Jeannin, Y. *J. Chem. Soc., Chem. Commun.* **1981**, 152.
(5) Herrmann, W. A. *Angew. Chem., Int. Ed. Engl.* **1982**, *21*, 117.
(6) Masters, C. *Adv. Organomet. Chem.* **1979**, *17*, 61.
(7) Brady III, R. C.; Pettit, R. *J. Am. Chem. Soc.* **1981**, *103*, 1287.
(8) (a) Herrmann, W. A. *Angew. Chem., Int. Ed. Engl.* **1978**, *17*, 800. (b) Herrmann, W. A. *Adv. Organomet. Chem.* **1982**, *20*, 159. (c) Herrman, W. A. *J. Organomet. Chem.* **1983**, *250*, 319.
(9) Hahn, J. E. *Prog. Inorg. Chem.* **1984**, *31*, 205.
(10) (a) Davies, D. L.; Dyke, A. F.; Knox, S. A. R.; Morris, M. J. *J. Organomet. Chem.* **1981**, *215*, C30; (b) Korswagen, R.; Ah, R.; Speth, D.; Ziegler, M. L. *Angew. Chem., Int. Ed. Engl.* **1981**, *20*, 1049.
(11) Schmidbauer, H. *Angew. Chem., Int. Ed. Engl.* **1983**, *22*, 907.
(12) (a) Hong, P.; Nishii, N.; Sonogashira, K.; Hagihara, N. *J. Chem. Soc., Chem. Commun.* **1972**, 993. (b) Yamamoto, T.; Garber, A. R.; Wilkinson, J. R.; Boss, C. B.; Streib, W. E.; Todd, L. J. *Ibid.* **1974**, 354.
(13) (a) Jones, R. A.; Wilkinson, G.; Gallas, A.; Hursthouse, K.; Malik, K. *J. Chem. Soc., Dalton Trans.* **1980**, 1771. (b) Dawkins, G. M.; Green, M.; Jeffrey, J. C.; Sambale, C.; Stone, F. G. A. *Ibid.* **1983**, 449. (c) Fischer, E. O.; Rustemeyer, P.; Orame, O.; Neugebauer, D.; Schubert, U. *J. Organomet. Chem.* **1983**, *247*, 7.
(14) Jones, R. A.; Wilkinson, G.; Galas, A. M. R.; Hursthouse, M. B.; Abdul-Malik, K. M. *J. Chem. Soc., Dalton Trans.* **1980**, 1771.
(15) (a) Theopold, K. H.; Bergman, R. G. *Organometallics* **1982**, *1*, 219. (b) Jacobsen, E. N.; Bergman, R. G. *Ibid.* **1984**, *3*, 329.
(16) Schmidbauer, H.; Schubert, U.; Jankik, P. *Angew. Chem., Int. Ed. Engl.* **1982**, *21*, 73.
(17) (a) Lin, Y. C.; Calabrese, J. C.; Wreford, S. S. *J. Am. Chem. Soc.* **1983**, *105*, 1679. (b) Yang, G. K.; Bergman, R. G. *Ibid.* **1983**, *105*, 6045.
(18) (a) Colburn, R. E.; Davies, D. L.; Dyke, A. F.; Endesfelder, A.; Knox, S. A. R.; Orpen, A. G.; Plaas, D. *J. Chem. Soc., Dalton Trans.* **1983**, 2661. (b) Colburn, R. E.; Dyke, A. F.; Knox, S. A. R.; Mead, K. A.; Woodward, P. *Ibid.* **1983**, 2099.

0002-7863/87/1509-3603$01.50/0 © 1987 American Chemical Society

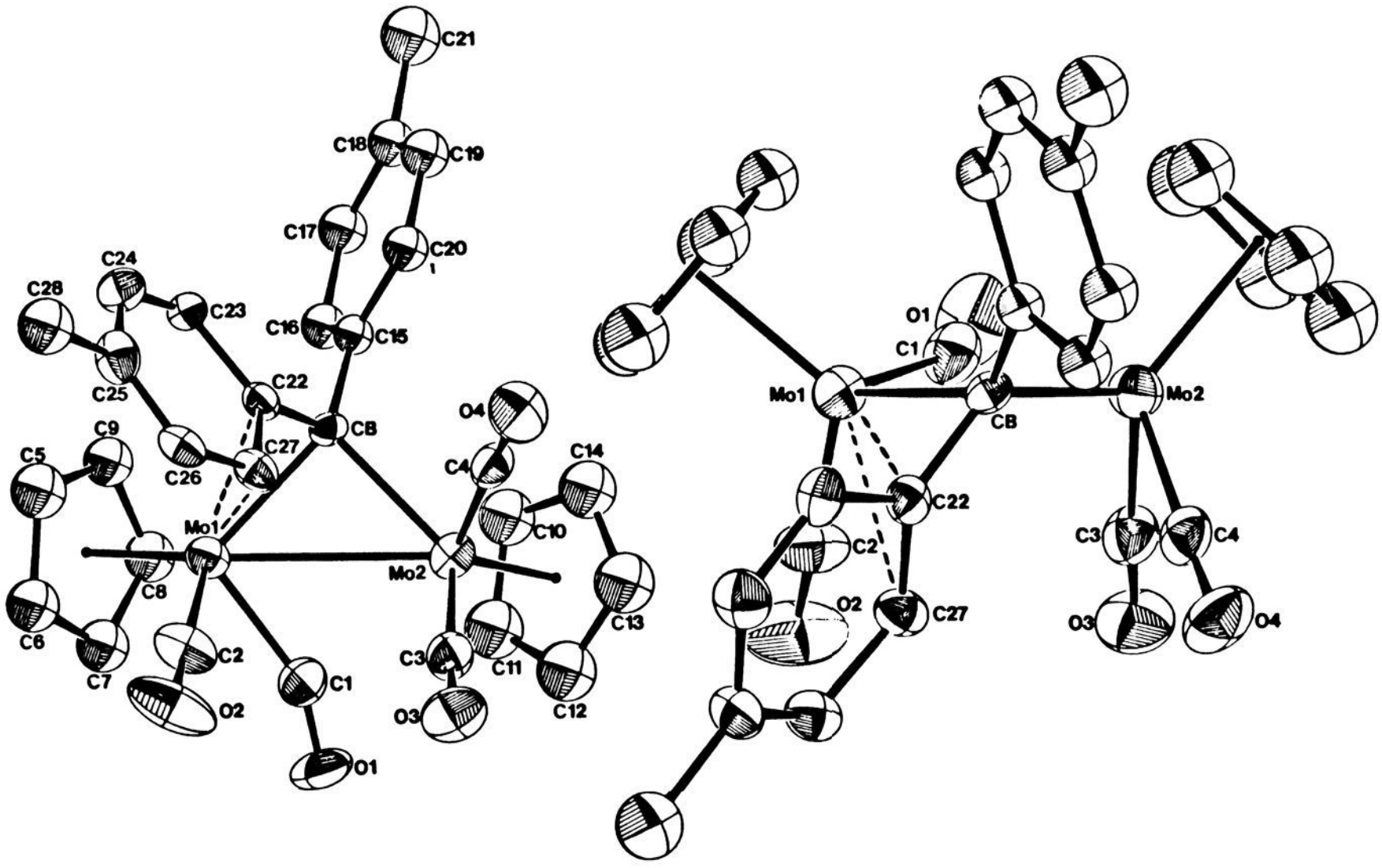

Figure 1. ORTEP drawings (50% ellipsoids) of $Cp_2Mo_2(CO)_4(\mu,\eta^3\text{-}C(p\text{-tolyl})_2)$, **2b**.

diazoalkanes with metal complexes with subsequent loss of dinitrogen.[8]

The last route, in particular, has been quite fruitful when applied to reactions involving complexes with multiple metal–metal bonding.[1,8,21] A previous paper[21] in this series described a group of diazoalkane adducts of $Cp_2Mo_2(CO)_4(Mo{\equiv}Mo)$ (**1**) and related multiply bonded dimers and their conversion into μ-alkylidene complexes **2**, $Cp_2Mo_2(CO)_4(\mu\text{-}CR_2)$. In this paper, we report the structure of two μ-alkylidenes of type **2**, their reactions with small molecules, e.g., CO, RNC, RCCR, and R_2CN_2, a kinetic study of the reaction of **2** (R = Ph) with CO, and an EHMO study of the electronic structure of these bridging alkylidenes. In addition, the crystal structure of a reaction product, from the reaction of **2** (CR_2 = fluorenylidene) with *i*-PrNC, is described.

Structural Results and Discussion

Structure of $Cp_2Mo_2(CO)_2(CAr_2)$. Previous studies[21,22] have shown that diphenyl- or di-*p*-tolyldiazomethane adducts of **1** decompose in an intramolecular reaction to the μ-diaryldiazomethane adducts **2a** (Ar = phenyl) or **2b** (Ar = *p*-tolyl). Presumably, the 1,3-dipolar cycloadduct **3** is an intermediate (eq 1, M = $Mo(CO)_2Cp$ or $Mo(CO)_2(C_5H_4Me)$ throughout this paper unless specified otherwise).

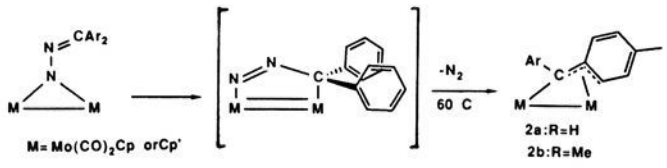

(1)

3

The crystal structure of **2b** shows that one of the aromatic rings is coordinated to one Mo atom in the manner indicated in eq 1. Figure 1 shows ORTEP plots of the molecule. Figure 3a is a view down the Mo2 → Mo1 bond vector. Table I lists selected bond distances and angles.

The Mo–Mo distance, 3.087 (2) Å, is appropriate for a Mo–Mo single bond. It has been argued elsewhere that the metal–metal bond order decreases by one unit for each pair of electrons added to the dimetal center in **1**.[23] The diarylmethylene group in **2b** is then donating a total of four electrons net to the Mo_2 center, two from the methylene and two from the coordinated phenyl ring. The methylene carbon bridges the two Mo atoms in a nearly symmetric manner, CB–Mo1 = 2.22 (1) and CB–Mo2 = 2.21 (1) Å. The pattern of the Mo1–C distances (Mo1–C22 = 2.22 (1), Mo1–C27 = 2.58 (1) Å) is very similar to that observed in a mononuclear π-benzyl complex of Mo, $Cp(CO)_2Mo(\eta^3\text{-}CH_2C_6H_4\text{-}p\text{-}Me)$.[24] Thus, the π-allyl type structure B shown below is an apt description of the Mo1–(μ-alkylidene) bonding. A similar structure has been observed in another μ-alkylidene formed in the ring-opening reactions of **1** with a cyclopropene.[26]

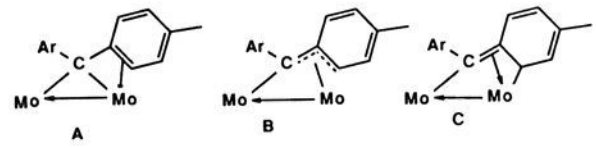

Structure B may be decomposed into the resonance extremes A and C shown above. The CB–C22 distance (1.44 (1) Å) is shorter than the CB–C15 distance (1.50 (1) Å) as expected for multiple bond character in the former bond, and the C–C bonds in the coordinated ring show definite alternations in bond lengths which are also consistent with the partial localization of double bond character as shown in C above. Thus, the average length of the C23–C24 and C25–C26 bonds is 1.36 (2) Å whereas the

(19) Bruce, M. I. *J. Organomet. Chem.* **1983**, *257*, 417; **1983**, *242*, 147
(20) (a) Ashworth, T. V.; Berry, M.; Howard, J. A. K.; Laguna, M.; Stone, F. G. A. *J. Chem. Soc., Dalton Trans.* **1980**, 1615. (b) Awang, M. R.; Jeffrey, J. C.; Stone, F. G. A. *Ibid.* **1983**, 2091
(21) Curtis, M. D.; Messerle, L.; D'Errico, J. J.; Butler, W. M.; Hay, M. S. *Organometallics* **1986**, *5*, 2283 and references therein.
(22) Messerle, L.; Curtis, M. D. *J. Am. Chem. Soc.* **1980**, *102*, 7789.
(23) Curtis, M. D.; Messerle, L.; Fotinos, N. A.; Gerlach, R. F. *ACS Symp. Ser.* **1981**, *155*, 221.
(24) (a) King, R. B.; Fronzaglia, A. *J. Am. Chem. Soc.* **1966**, *88*, 709. (b) Cotton, F. A.; LaPrade, M. D. *Ibid.* **1968**, *90*, 5418.
(25) Mead, K. A.; Moore, I.; Stone, F. G. A.; Woodward, P. *J. Chem. Soc., Dalton Trans.* **1983**, 2083.
(26) Barker, G. K.; Carroll, W. E.; Green, M.; Welch, A. J. *J. Chem. Soc., Chem. Commun.* **1980**, 1071.

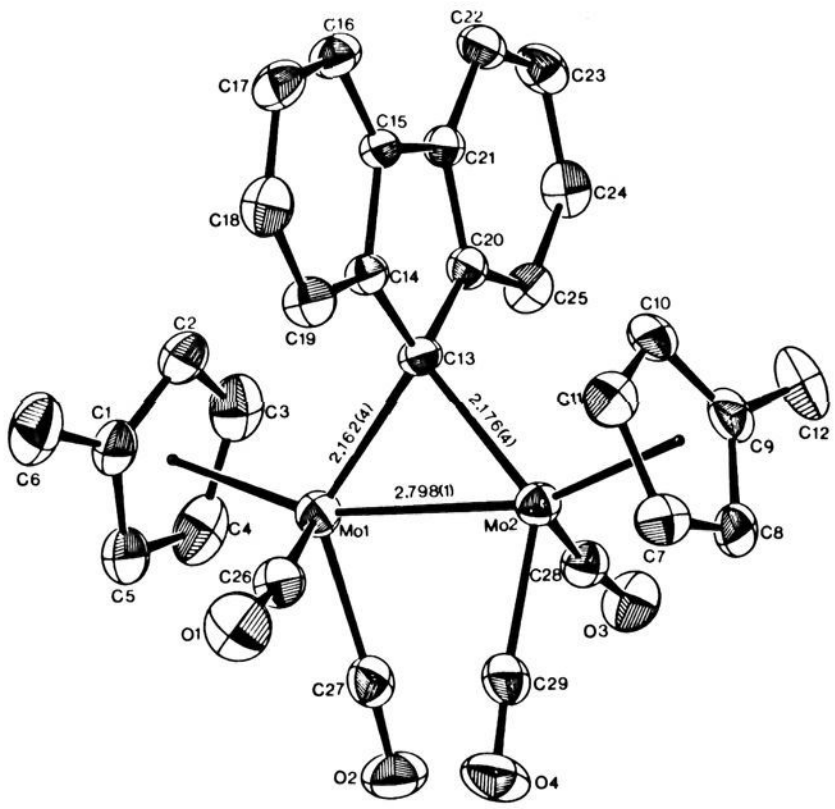

Figure 2. ORTEP drawing (50% ellipsoids) of $Cp_2Mo_2(CO)_4(\mu$-fluorenylidene), **2c**.

average of the remaining ring C–C bond distances is 1.44 (2) Å.

The formal electron distribution in **2a** or **2b** is interesting. If the Ar_2C ligand is counted as a dianion, then each molybdenum in **2a** or **2b** has a formal 2+ oxidation state. The Mo1 coordination sphere is essentially identical with a $CpMo(CO)_3(\pi$-allyl) and Mo1 has an 18-electron count. Mo_2, on the other hand, has the same coordination sphere as $CpMo(CO)_2R$ and has only a 16-electron count. It is therefore proposed that Mo1 donates two electrons to Mo2 in a dative Mo1 → Mo2 bond. Thus, Mo1 has a formal 1+ charge and Mo2 has formal 1− charge. The role of the semibridging carbonyl (Figure 1) is then understood to draw off excess electron density from Mo2.[27]

Structure of $Cp_2Mo_2(CO)_4(\mu$-$CC_{12}H_8)$ (2c). To prevent one phenyl ring from coordinating to the dimetal center as was observed in **2a** or **2b**, the rings were effectively tied together with a C–C bond by using 9-diazofluorene in place of diphenyl- or di-*p*-tolyldiazomethane (eq 2).[21,28] In this reaction, an intermediate diazoalkane adduct was not observed. Presumably, lessened steric congestion in the 1,3-dipolar cycloadduct intermediate **4**, as compared to **3**, permits a more facile loss of N_2.

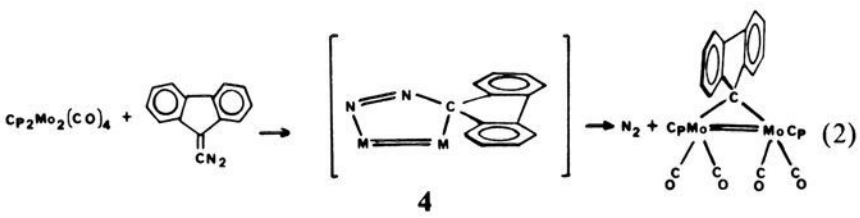

4

Figure 2 presents an ORTEP of **2c** with the numbering scheme. Figure 3b shows a view of the molecule down the Mo–Mo bond. Selected bond distances and angles are collected in Table II. As expected, the aryl rings of the μ-fluorenylidene ligand are not bonding to the Mo atoms. The fluorenylidene thus donates two electrons net to the dimetal center, and the Mo–Mo bond order is reduced 3 → 2 in going from **1** → **2c**. The Mo═Mo distance, 2.798 (1) Å, lies nearly midway between the Mo≡Mo triple bond distance (2.448 (1) Å) in **1** and the Mo–Mo single bond distance in $Cp_2Mo_2(CO)_6$ (3.235 (1) Å).[29] The Mo═Mo distance in **2c** is very similar to the Mo═Mo bond length (2.745 (2) Å) in **5** ($Cp^* = C_5Me_5$).[30] Other dimetallacyclopropenes have been synthesized,[8,15,31] but complex **2c** is the only one with no other ligands bridging the M═M bond.

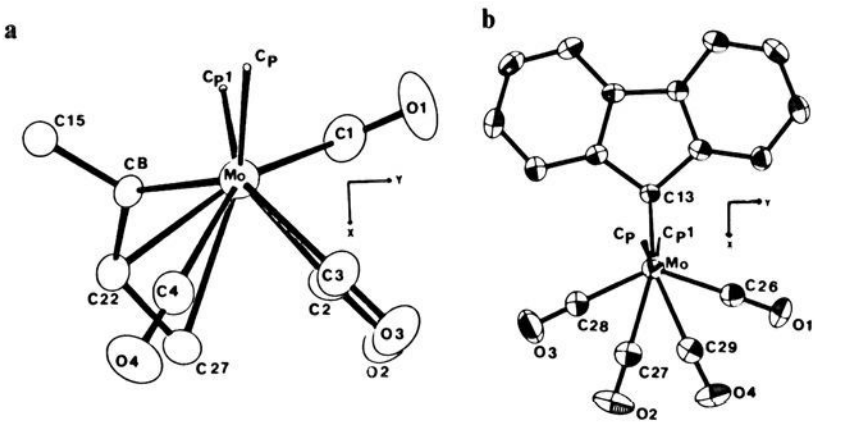

Figure 3. ORTEP drawings showing the relative orientations of the bridging alkylidene carbons in **2b** (a) and **2c** (b). The view is down the Mo–Mo bond. The phenyl carbons (C22, C27) bonded to Mo in **2b** are included in the drawing of **2b**.

Table II. Selected Bond Distances and Angles for **2c**

bond	distance (Å)	bond	distance (Å)
Mo1–C26	1.943 (4)	C13–C14	1.479 (6)
Mo1–C27	2.007 (5)	C13–C20	1.497 (5)
Mo1–C13	2.162 (4)	C26–O1	1.152 (5)
Mo1–Mo2	2.798 (1)	C27–O2	1.134 (5)
Mo2–C28	1.946 (5)	C28–O3	1.156 (5)
Mo2–C29	2.016 (5)	C29–O4	1.132 (5)
Mo2–C13	2.176 (4)		
bond	**angle (deg)**	**bond**	**angle (deg)**
C26–Mo1–C27	86.65 (18)	C14–C13–Mo1	117.19 (28)
C26–Mo1–C13	96.52 (16)	C14–C13–Mo2	119.31 (27)
C26–Mo1–Mo2	76.26 (13)	C20–C13–Mo1	119.49 (26)
C27–Mo1–C13	132.89 (16)	Mo1–C13–Mo2	80.34 (13)
C27–Mo1–Mo2	86.01 (13)	O1–C26–Mo1	168.59 (36)
C13–Mo1–Mo2	50.04 (11)	O2–C27–Mo1	174.22 (40)
C28–Mo2–C29	88.34 (18)	O3–C28–Mo2	168.62 (41)
C28–Mo2–C13	97.31 (17)	O4–C29–Mo2	174.13 (39)
C28–Mo2–Mo1	75.81 (14)	C13–Mo2–Mo1	49.62 (10)
C29–Mo2–Mo1	86.30 (13)	C20–C13–Mo2	117.90 (94)
C14–C13–C20	102.78 (32)		

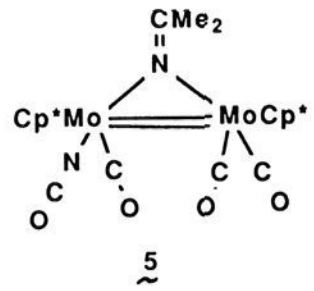

5

The μ-fluorenylidene ligand is essentially perpendicular to the Mo═Mo bond and is symmetrically bonded to the two Mo atoms. The average Mo–C distance (2.17 (1) Å) is somewhat shorter than the Mo–CB average distance in **2b** (2.21 (1) Å). The Mo–C bonding may be slightly stronger in **2c** because the bridging group is not skewed by the molybdenum–ring interaction as it is in **2b**. The Mo–C13–Mo angle, 80.3 (1)°, in **2c** is also smaller than the Mo–CB–Mo angle, 88.4 (4)°, in **2b** as a consequence of the shorter Mo–Mo bond in the former compound. The bond angles and distances in the remainder of the fluorenylidene ligand are identical within experimental error to those in free fluorene.[32]

As Figure 3 shows, the disposition of the Cp and CO ligand spheres in **2b** and **2c** differ substantially as a result of the η^3-benzylic interaction present in **2b**. The bridging carbon, CB, in **2b** lies in the *yz*-plane more or less perpendicular to the mean plane (*xz*) containing the Mo atoms and Cp centroids, whereas the bridging carbon atom, C_{13}, in **2c** lies in the *xz*-plane. The carbonyl groups in **2b** are skewed around to make room for the η^3-benzylic

(27) (a) Morris-Sherwood, B. J.; Powell, C. B.; Hall, M. B. *J. Am. Chem. Soc.* **1984**, *106*, 5079. Cotton, F. A.; Kruczynski, L.; Frenz, B. A. *J. Organomet. Chem.* **1978**, *160*, 93.
(28) D'Errico, J. J.; Curtis, M. D. *J. Am. Chem. Soc.* **1983**, *105*, 4479.
(29) Adams, R. D.; Collins, D. M.; Cotton, F. A. *Inorg. Chem.* **1974**, *13*, 1086.
(30) Herrmann, W. A.; Bell, L. K.; Ziegler, M. L.; Pfisterer, K.; Dahl, C. *J. Organomet. Chem.* **1983**, *247*, 39.
(31) Dimas, P. A.; Shapley, J. R. *J. Organomet. Chem.* **1982**, *228*, C2.
(32) Burns, D. M.; Hall, J. *Proc. Roy. Soc.* **1955**, *A227*, 200.

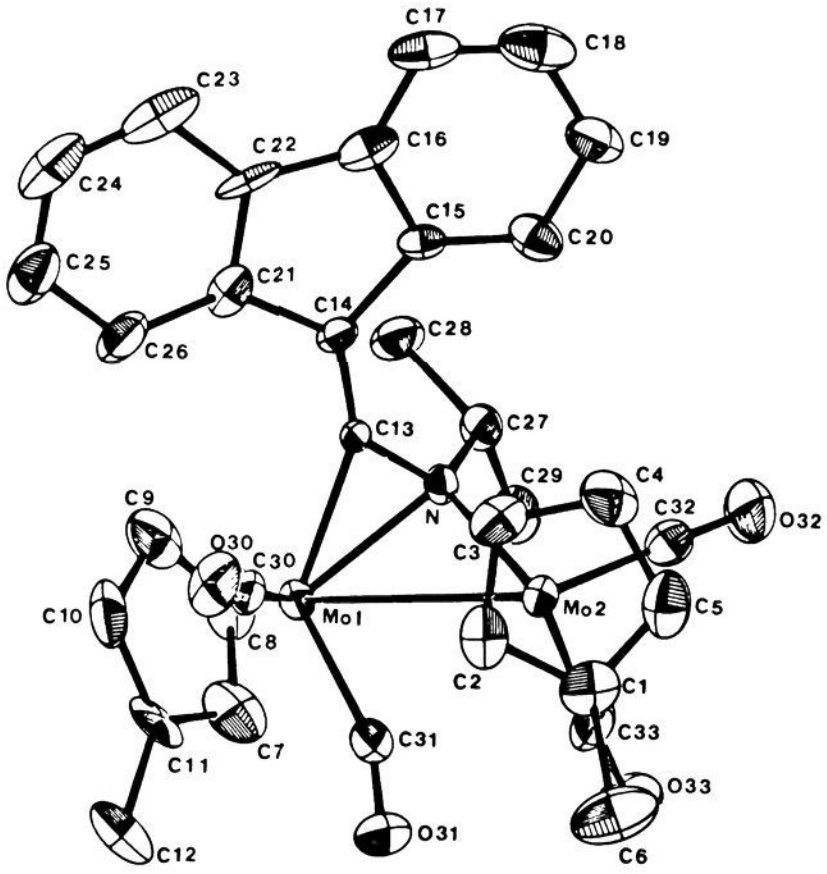

Figure 4. ORTEP drawing (50% ellipsoids) of $Cp_2Mo_2(CO)_4(\mu,\eta^1,\eta^2\text{-}i\text{-}PrNC{=}CC_{12}H_8)$, **8**.

bonding in **2b**, but they are symmetrically placed in **2c** (the effective symmetry of **2c** is C_2). The relative positions of the μ-alkylidene in **2b** and **2c** have a strong influence on the reactivities of these compounds (see below).

The carbonyl groups in **2c** may be grouped into two types: those nearly trans to the fluorenylidene ligand (C27–O2 and C29–O4) and those cis to it (C26–O1 and C28–O3). The average Mo–CO (trans) distance (2.012 (5) Å) is longer than the average Mo–CO (cis) distance (1.945 (5) Å). The trans CO ligands back-bond with the π_{xz} orbital of the Mo_2 fragment. However, this orbital is stabilized by its interaction with the μ-fluorenylidene ligand and the π-back-bonding is not as effective as with the cis CO ligands which bond to the π_{yx} Mo_2 orbital. Computed Mo–CO overlap populations are 0.79 for trans and 0.90 for cis CO ligands (see below).

Structure of $Cp_2Mo_2(CO)_3(CAr_2)(N_2Car_2)$ (6). The μ-alkylidenes **2a** or **2b** react with Ar_2CN_2 to give the *terminal* alkylidene complex **6** (eq 3). The structure of **6** has been confirmed by a single-crystal X-ray study, and the details of the structure and the fluxional behavior of **6** will be reported elsewhere. A preliminary report has appeared.[33]

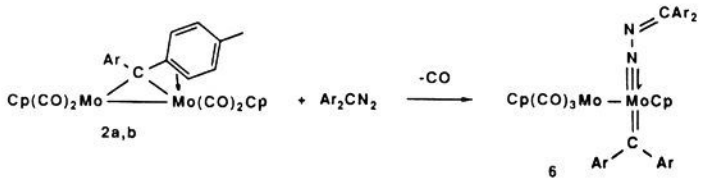

(3)

In the course of the reaction shown in eq 3, one carbonyl has been transferred across the Mo–Mo bond, giving a $CpMo(CO)_3$ unit, the μ-alkylidene moiety has shifted to a terminal position and bonds to only one Mo atom, and the diazoalkane has displaced the remaining CO.

Structure of $Cp_2'Mo_2(CO)_3(CN\text{-}i\text{-}Pr)(\mu\text{-}\eta^1,\eta^2\text{-}i\text{-}PrNC{=}C_{13}H_8)$ (8, Cp′ = C_5H_4Me). The μ-fluorenylidene complex **2c** reacted with isopropyl isonitrile to give a mixture of products, from which a 20% yield of complex **7** was isolated by fractional crystallization.

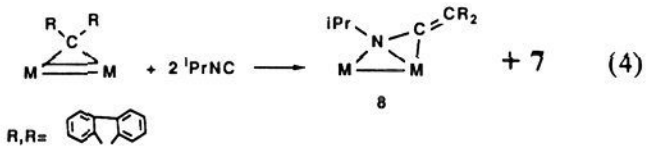

(4)

Attempts to grow crystallographic quality crystals of **7** were unsuccessful. However, one well-formed crystal was found in one attempt, and upon solution of the crystal structure, the molecule was found to be complex **8**. Complexes **7** and **8** differ only in that **7** has a terminal carbonyl replaced by a terminal isonitrile (ν_{CN} = 2120 cm^{-1}, see Experimental Section for further spectroscopic details). Apparently, **8** was present as a trace impurity in the sample of **7**.

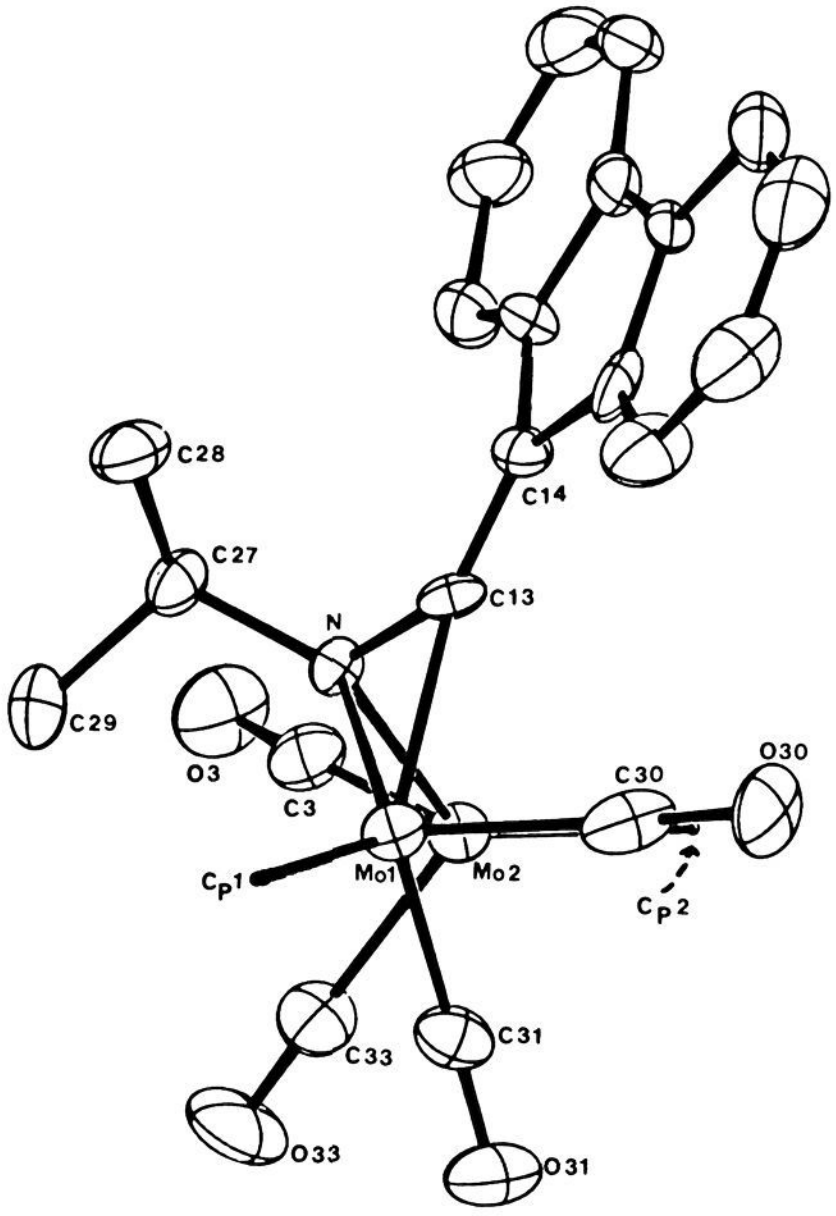

Figure 5. ORTEP drawing of **8** viewed approximately down the Mo–Mo bond.

Chart I

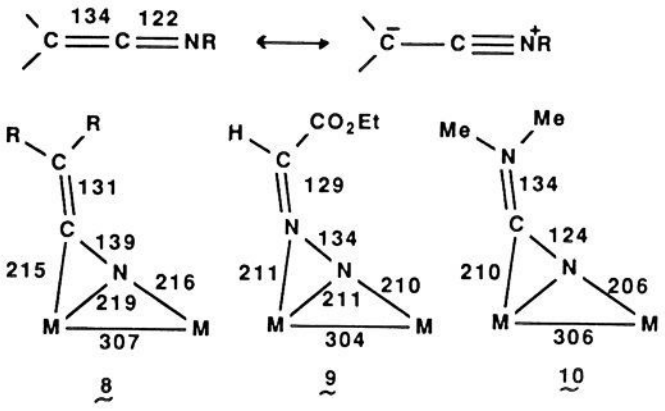

The structure of **8** (Figures 4 and 5 and Table III) shows that the fluorenylidene fragment has been displaced from bonding contact with the metals and that the isonitrile has coupled to the fluorenylidene fragment to form a keteneimine ligand. The keteneimine is bonded to the dimetal framework in a $\mu\text{-}\eta^2(N),\eta^1(C)$ fashion and donates a total of four electrons to the M_2 unit. As a result, the M–M bond order is decreased from 3 in the free M_2 unit to 1 in the keteneimine adduct. The Mo–Mo distance, 3.067 (1) Å, is consistent with a metal–metal single bond.

The bonding within the coordinated keteneimine[34] may be compared to that in free keteneimines and in related $\mu\text{-}\eta^2,\eta^1$

(33) Messerle, L.; Curtis, M. D. *J. Am. Chem. Soc.* **1982**, *104*, 889.

(34) Runge, W. In *The Chemistry Ketenes, Allenes, and Related Compounds*; Patai, S., Ed.; Interscience: New York, 1980; pp 60–61.

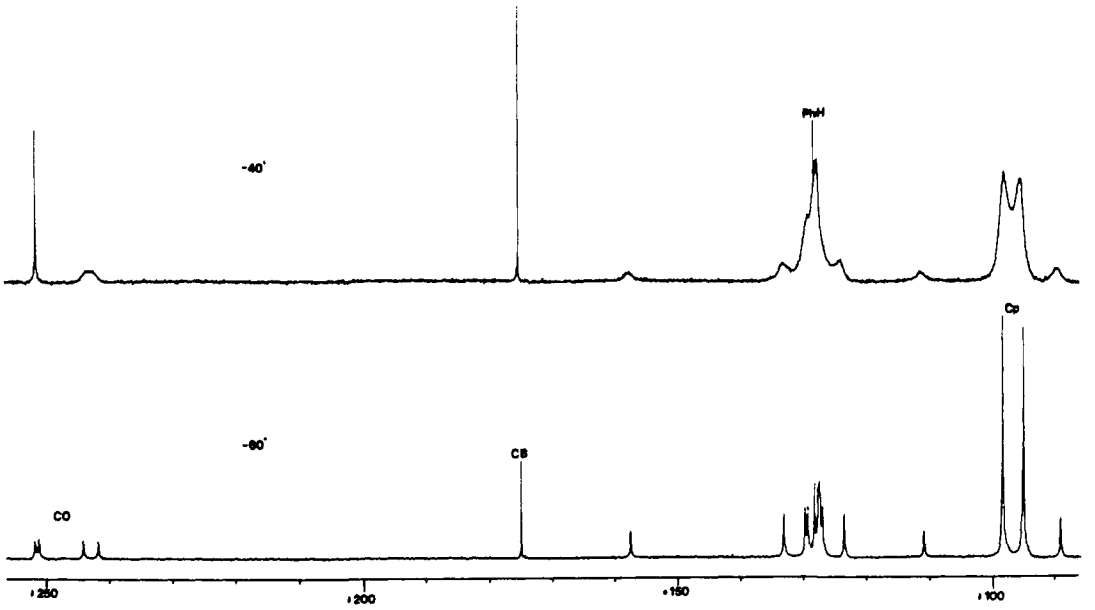

Figure 6. ^{13}C NMR spectra of $Cp_2Mo_2(CO)_4(\mu,\eta^3\text{-}CPh_2)$, **2a**, at −40 °C (top) and −60 °C (bottom).

adducts of the M_2 core. The latter include adducts of ethyl diazoacetate **9**[21] and *N,N*-dimethylcyanamide **10**[35] (Chart I, bond distances in pm).

In free keteneimines, the C–N bond has a formal bond order (BO) of ca. 2.3 due to the resonance depicted in the chart. Upon coordination to the M_2 unit, the observed C–N distance, 1.39 (1) Å, is indicative of a BO of ca. 1.3. The adduct **9** of the electronically similar diazoacetate shows a similar pattern of bond orders: C≡N ca. 2.0 and N–N ca. 1.2. The C–N bond order of the coordinated Me_2N—C≡N ligand falls to ca. 2.3 from a value of around 3 in the free ligand. A Mo–N distance around 2.1 Å in these types of compounds indicates the presence of some π-bonding (BO 1.2).[21]

The overall structure of **8** bears a striking resemblance to the adduct of ethyl diazoacetate with $Cp^*_2Mo_2(CO)_4$.[21]

NMR and Solution Dynamics. $M_2(\mu\text{-}CAr_2)$. The μ-diarylmethylene complexes **2a** and **2b** are fluxional in solution. At room temperature, the ^1H NMR spectrum of **2a** has a single peak at δ 4.70 due to the Cp protons, triplets at δ 6.90 and 6.69 (J = 8 Hz) due to the meta and para protons, respectively, and a very broad "singlet" at δ 6.54 due to the ortho protons. The room temperature ^{13}C NMR shows a singlet for the Cp carbons at δ 96.9, a broad hump assigned to the ortho carbons at δ 120.1, sharp peaks at δ 125.7 and 129.3 (meta and para carbons) and 176.0 (alkylidene carbon), and two carbonyl carbon resonances at δ 242.8 and 251.2. Thus, at room temperature, the Cp groups are equivalent, as are the two phenyl rings. Furthermore, the two sides of the phenyl rings are equivalent and appear as a simple pattern expected for C_6H_5X. The four carbonyls appear as two sets.

At −60 °C, however, the ^{13}C NMR spectra of **2a** and **2b** are consistent with the solid-state structure (Figure 6). Each compound gives four peaks for the four carbonyls between δ 242 and 252. The peak due to the bridging alkylidene carbon (CB) is at δ 174.8 (177.0) (the first value is for **2a**, the second value in parentheses is for **2b**). The Cp groups are inequivalent and resonate at δ 98.3 (98.2) and 95.1 (94.5). The aryl methyl carbon atoms of **2b** are also inequivalent and give peaks at δ 21.0 and 20.5.

The chemical shifts of the aryl carbons are spread out over a much larger range of values than is normally observed. Thus, peaks at δ 88.9 (92.2), 111.0 (107.9), 123.3 (137.5), 133.1 (132.8), and 157.5 (154.6) are observed for **2a** and **2b**. With the exception of the peak at δ 92.2 (J_{CH} = 167 Hz), these peaks remain singlets in gated decoupled spectra of **2b**. The peak at highest field is assigned to the ortho carbon bonded to Mo on the basis of its π-allylic character, the fact that the terminal carbon of a π-allyl group is shifted the farthest upfield[36] and the observed J_{CH}. The peaks at 111.0 (107.9) are assigned to the ipso carbon bonded to Mo also on the basis of its π-allylic character. The peaks farthest downfield at 157.5 (154.6) are assigned to the para carbons of the complexed ring, and their large chemical shifts

Table III. Selected Bond Distances and Angles for **8**

bond	distance (Å)	bond	distance (Å)
Mo1–Mo2	3.069 (1)	C13–C14	1.319 (11)
Mo1–C13	2.133 (9)	C13–N1	1.386 (10)
Mo1–C30	1.938 (13)	C14–C15	1.501 (12)
Mo1–C31	1.989 (11)	C14–C21	1.480 (12)
Mo1–N1	2.196 (7)	C27–N1	1.500 (11)
Mo2–C13	2.914 (8)	C30–O30	1.154 (13)
Mo2–C31	2.664 (10)	C31–O31	1.166 (10)
Mo2–C32	1.931 (12)	C32–O32	1.166 (11)
Mo2–C33	1.940 (11)	C33–O33	1.134 (11)
bond	**angle (deg)**	**bond**	**angle (deg)**
Mo2–Mo1–C13	65.3 (2)	Mo1–C13–Mo2	73.1 (2)
Mo2–Mo1–C30	87.2 (3)	Mo1–C13–C14	151.1 (7)
C13–Mo1–C31	78.0 (4)	Mo2–C13–C14	128.8 (6)
Mo2–Mo1–C31	59.0 (3)	Mo1–C13–N1	73.8 (5)
C13–Mo1–C31	121.0 (4)	Mo2–C13–N1	44.5 (4)
Mo2–Mo1–N1	44.6 (2)	C14–C13–N1	134.5 (8)
C13–Mo1–N1	37.3 (3)	C13–C14–C15	128.1 (8)
C30–Mo1–N1	106.4 (4)	C13–C14–C21	127.1 (9)
C31–Mo1–N1	101.9 (3)	C15–C14–C21	104.7 (8)
Mo1–Mo2–C13	41.7 (2)	C28–C27–C29	110.8 (8)
Mo1–Mo2–C31	39.8 (2)	C28–C27–N1	114.2 (7)
C13–Mo2–C31	79.9 (3)	C29–C27–N1	111.5 (8)
Mo1–Mo2–C32	124.7 (4)	Mo1–C30–O30	176.9 (9)
C13–Mo2–C32	107.2 (3)	Mo1–C31–Mo2	81.2 (3)
C31–Mo2–C32	137.1 (4)	Mo1–C31–O31	160.1 (9)
Mo1–Mo2–C33	95.5 (3)	Mo2–C31–O31	118.4 (8)
C13–Mo2–C33	130.3 (4)	Mo2–C32–O32	177 (1)
C31–Mo2–C33	70.3 (4)	Mo2–C33–O33	175 (1)
C32–Mo2–C33	74.0 (4)	Mo1–N1–Mo2	89.7 (3)
Mo1–Mo2–N1	45.7 (2)	Mo1–N1–C13	68.9 (4)
C13–Mo2–N1	26.8 (2)	Mo2–N1–C13	108.8 (5)
C31–Mo2–N1	84.2 (3)	Mo1–N1–C27	127.0 (6)
C32–Mo2–N1	86.1 (3)	Mo2–N1–C27	125.4 (5)
C33–Mo2–N1	109.4 (4)	C13–N1–C27	121.0 (7)

(35) Chisholm, M. H.; Cotton, F. A.; Extine, M. W.; Rankel, L. A. *J. Am. Chem. Soc.* **1978**, *100*, 807.

(36) Jolly, P. W.; Mynott, R. *Adv. Organomet. Chem.* **1981**, *19*, 257.

Scheme I

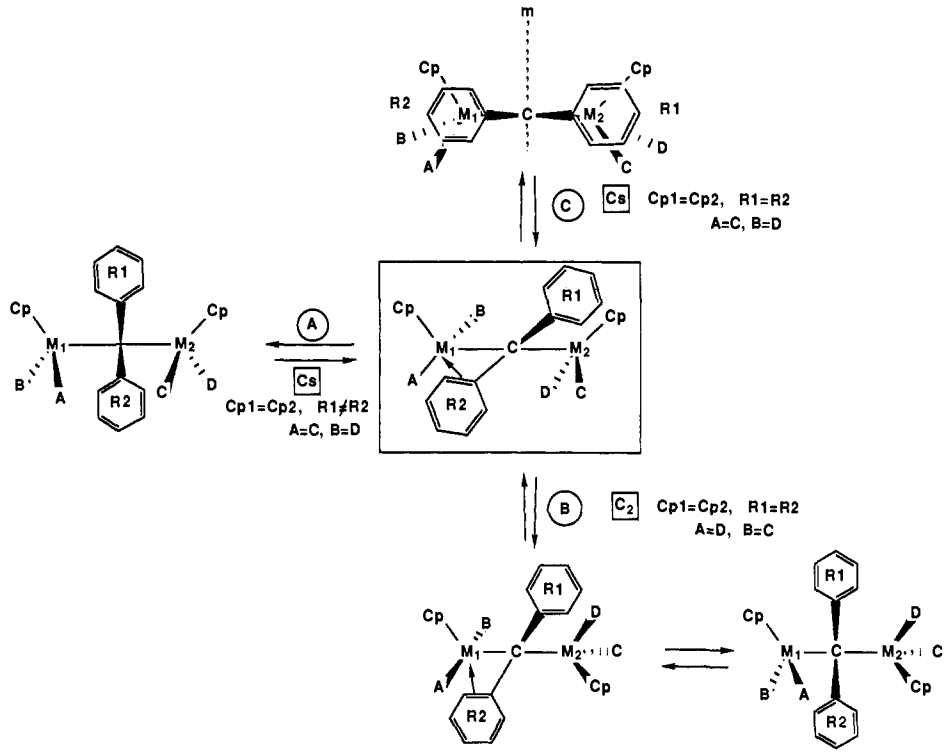

reflect the localization of the double bonds in the complexed aryl group (see above). The resonances at δ 133.1 (132.8) and 123.3 (137.5) are assigned to the ipso and para carbons of the uncomplexed aryl group, respectively. The remaining ortho and meta aryl carbon resonances are bunched in the usual range, δ 126–130, and split into doublets in gated decoupled spectra ($J \approx 160$–170 Hz).

At −40 °C, all peaks show the broadening effects caused by the onset of fluxional motion (the two lowest field carbonyl peaks have already merged at this temperature—see top spectrum in Figure 6). The activation energy for the fluxional process was estimated to be ca. 10 kcal/mol from the coalescence temperature for the Cp peaks. Possible fluxional processes are shown in Scheme I. The highest effective symmetry in the fast exchange limit is either C_2 or C_s. If it is C_s, then the phenyl rings must be symmetry related (i.e., the ring centroids cannot lie in the mirror plane). Thus, a process, e.g., path A in Scheme I, in which the coordinated ring is detached from the metal and is reattached at the other metal produces effective C_s symmetry which averages the environments of the Cp groups, gives two sets of carbonyls (A ↔ C, B ↔ D), but leaves the phenyl rings inequivalent. Therefore, path A does not account for the high-temperature spectra. Note: rapid rotation of the phenyl rings about the C(ipso)–CB bond is assumed at higher temperatures.

Path B (Scheme I) depicts a mechanism in which the coordinated ring is detached and one end of the dimetal fragment is rotated about the Mo–Mo bond to give a trans structure with C_2 symmetry. This mechanism averages the Cp ring environments and the phenyl ring environments and gives two sets of carbonyls (A ↔ D, B ↔ C).

Since path A involves less atomic motion than path B, it is difficult to imagine the latter occurring without the former. Sequential traversal of both paths A and B produces effective C_{2v} symmetry (i.e., all carbonyls become equivalent—see below). Since effective C_{2v} symmetry is not observed, path B is probably not responsible for the observed averaging of magnetic environments in the fluxional process.

An alternate path which gives the correct average structure is depicted in path C, Scheme I. In this path, the alkylidene fragment twists around to give an intermediate with effective C_s symmetry. Normally, such a twisting motion would be a high-energy process since an important component of the metal–bridge bond is broken.[37] In this case, however, bonding contributions, e.g., D and E, below, may stabilize this pathway which gives

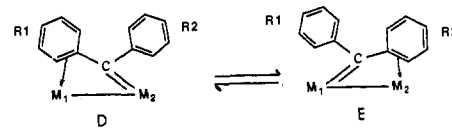

D E

equivalent Cp's and equivalent phenyl rings and divides the carbonyls into two sets, A ↔ C, B ↔ D. Sequential traversal of paths A and C merely averages the environments of the Cp and CO groups at a faster rate than path C alone but does not lead to higher effective symmetry. A related fluxional process involving a bridge ⇄ terminal alkylidene conversion has been observed by Dyke et al.[38]

$(C_5H_4Me)_2(CO)_4Mo_2(\mu\text{-}CC_{12}H_8)$ (2c′). At 30 °C, the ^1H NMR spectrum of **2c′** showed a single A_2B_2 pattern centered at δ 4.11 ($\Delta\delta$ = 112 Hz, J_{AB} = 2.4 Hz) for the Cp protons, a singlet at δ 1.18 for the Cp-methyl protons, and an ABCD pattern for the protons on the fluorenylidene ligand. The ^{13}C NMR spectrum showed a singlet for the carbonyl carbons at δ 236.1 and a singlet at δ 164.5 for the alkylidene carbon.

The virtual C_2 symmetry observed for **2c′** in the solid state requires two types of carbonyls, and the Cp′(C_5H_4Me) protons should be diastereotopic. At −61 °C, the A_2B_2 pattern collapsed to an ABCD pattern as expected on the basis of the solid-state structure. Unfortunately, the low solubility of **2c′** precluded the collection of a low-temperature ^{13}C NMR spectrum.

Thus, the fluxional process interconverts enantiomers and gives rise to effective C_{2v} symmetry at ambient temperature. The minimal motion process which accomplishes this interconversion is shown below (the horizontal line represents the plane of the fluorenylidene group).

Presumably, the bulk of the phenyl groups in **2a** or **2b** precludes transition states, e.g., F, which would give rise to effective C_{2v}

(37) (a) Hofmann, P. *Angew. Chem., Int. Ed. Engl.* **1979**, *18*, 554. (b) Pinhas, A. R.; Albright, T. A.; Hofmann, P.; Hoffmann, R. *Helv. Chim. Acta* **1980**, *63*, 29. (c) Calabro, D. C.; Lichtenberger, D. L.; Herrmann, W. A. *J. Am. Chem. Soc.* **1981**, *103*, 6852.

(38) Dyke, A. F.; Knox, S. A. R.; Mead, K. A.; Woodward, P. *J. Chem. Soc., Chem. Commun.* **1981**, 861.

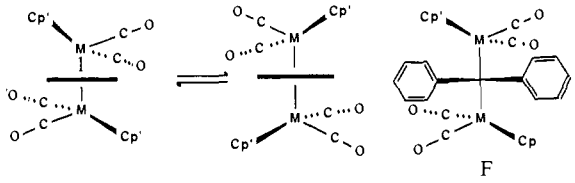

F

symmetry in the fast-exchange NMR spectra of the $M_2(CAr_2)$ complexes.

Reactions of the Bridging Alkylidenes 2a–2c. As pointed out in the introduction, bridging alkylidenes have been proposed as intermediates in a variety of catalytic reactions. We have therefore investigated the reactions of the bridging alkylidenes **2a–2c** with a variety of small molecules encountered in various catalytic cycles proposed to involve μ-alkylidenes. The reactivity characteristics of alkylidene intermediate(s) may then be understood in comparison to the behavior of isolable alkylidene complexes.

With H_2/D_2. The diaryl alkylidenes **2a** or **2b** react with H_2 to regenerate the triply bonded dimer, $Cp_2Mo_2(CO)_4$, and the diarylmethane, Ar_2CH_2. With pure D_2 as reactant, only two D atoms were incorporated in the product diarylmethane (MS), and ^2D NMR showed exclusive incorporation on the alkylidene carbon as evidenced by a single peak at δ 3.71, i.e., no D scrambling into the aryl ring positions was observed. Thus, Ar_2CD_2 was the sole organic product.

When **2b** was allowed to react with a 1:1 mixture of $H_2 + D_2$ (99.99%), an MS analysis of the resulting di-*p*-tolylmethane gave an observed ratio of $Ar_2CH_2/Ar_2CHD/Ar_2CD_2$ of approximately 6.1:1.0:3.9 (a fully satisfactory fit of the line intensities could not be obtained, possibly due to differential fragmentation rates of Ar_2CH_2 vs. Ar_2CD_2). Thus, the approximate kinetic isotope effect $k_{H_2}/k_{D_2} = 1.6$. The ^2D NMR spectrum of the product, however, showed only a single sharp peak corresponding to Ar_2CD_2 (control experiments established that J_{HD} in Ar_2CHD would have been resolved). Thus, the concentration of Ar_2CHD, if present, was below the detection limit of the ^2D NMR experiment. Since a completely self-consistent fit of the MS line intensities was not obtained, we are inclined to believe that little, if any, scrambling occurs in the H_2/D_2 reaction, which is then best represented by eq 5.

$$M_2(\mu\text{-}CAr_2) + H_2/D_2 \xrightarrow[4atm]{50\ ^\circ C} Ar_2CH_2 + Ar_2CD_2 + M{\equiv}M \quad (5)$$

The reaction of the μ-fluorenylidene complex **2c** with H_2 was considerably more sluggish. A higher H_2 pressure and longer reaction times were required (eq 6).

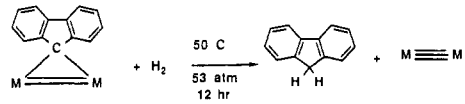

(6)

With CO. The reaction of the μ-alkylidene **2a** with CO is complex, and the detailed course of the reaction depends on the temperature and CO pressure. Figure 7 shows the changes in the CO stretching region as a function of time at 27 °C and P_{CO} = 1 atm. The intensity of the peaks due to **2a** at 1830 and 1780 cm^{-1} decreases smoothly and follows pseudo-first-order kinetics for a constant P_{CO} (Figure 8). New peaks at 2040 and 2000 cm^{-1} begin to grow concurrently, but then their intensities remain nearly constant after 1 half-life. A shoulder at 1865 cm^{-1} is prominent at low CO pressures, is less prominent at higher CO pressures, and begins to disappear as the starting material is consumed (after ca. 1 half-life). A weak signal due to diphenyl ketene at 2080 cm^{-1} begins to grow after 1 half-life and then decreases. At higher CO pressures (3 atm) and temperature (60 °C), diphenyl ketene is a major product. At lower CO pressures and lower temperatures, it is a minor product. The strong peaks at 1940 and 1900 cm^{-1} are due to the overlapping peaks of the starting complex **2a**, the final, isolated organometallic product, $Cp_2Mo_2(CO)_6$, and possibly of unidentified intermediates. A shoulder at 1955 cm^{-1} is seen only at higher CO pressures and grows faster when all the starting material is consumed.

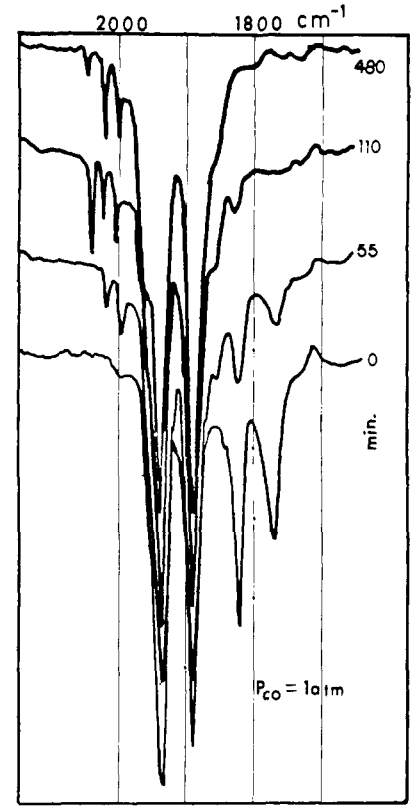

Figure 7. IR spectra as a function of time of a toluene solution of $Cp_2Mo_2(CO)_4(\mu,\eta^3\text{-}CPh_2)$, **2a**, reacting with CO (P = 1 atm.).

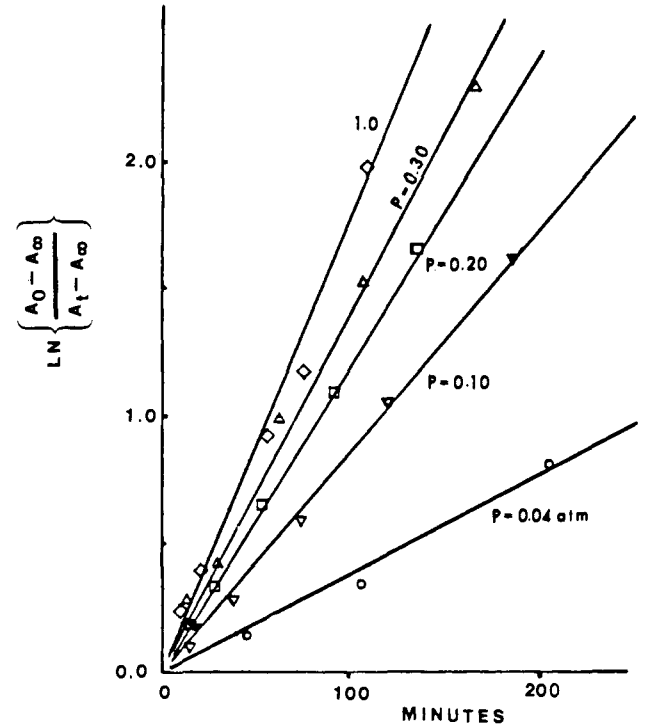

Figure 8. Pseudo-first order plots of ln(absorbance) at 1780 cm^{-1} vs. time (min) for the reaction of $Cp_2Mo_2(CO)_4(\mu,\eta^3\text{-}CPh_2)$, **2a**, with CO as a function of CO pressure.

A ^1H NMR study of the reaction showed $Cp_2Mo_2(CO)_6$ was formed rapidly and was the major product (75%) at 27 °C and P_{CO} = 0.3 atm. A second signal at δ 5.0 due to Cp groups of an unidentified compound (25%) was observed. The ratio of the signal intensities due to $Cp_2Mo_2(CO)_6$ and the unidentified complex remained constant throughout the reaction. The unknown compound constituted ca. 50% of the product at P = 0.2 atm. This unidentified product decomposed upon attempts to separate and

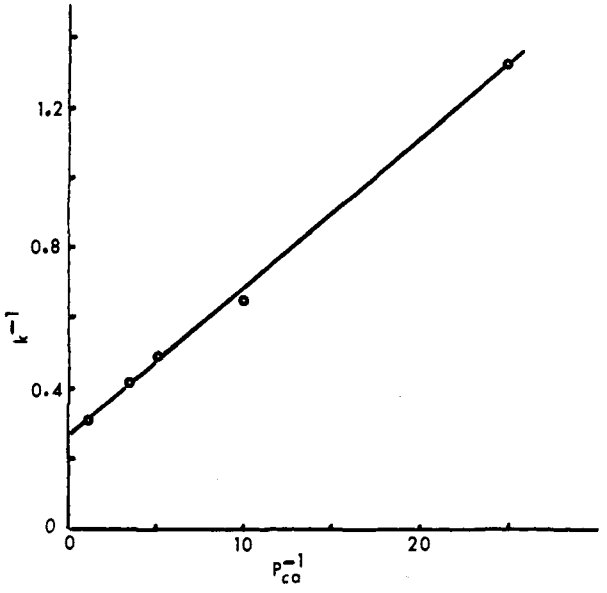

Figure 9. Reciprocal of the observed, pseudo-first order rate constant vs. the reciprocal of the CO pressure in the reaction of $Cp_2Mo_2(CO)_4(\mu,\eta^3\text{-}CPh_2)$ with CO.

purify it. No other signals were observed in the Cp region of the spectrum.

Several control experiments were conducted. Diphenyl ketene did not react at room temperature with triply bonded **1** or with $Cp_2Mo_2(CO)_6$ after 17 h. No reaction with these reagents was observed after 6 h at 60 °C. The ketene did not react with **2a** after 17 h at 27 °C. However, a reaction was noted (ca. 80% conversion of the ketene and ca. 50% conversion of **2a**) after 6 h at 60 °C. New peaks in the CO region were found at 2040, 1950, and 1860 cm^{-1}. This product was not identified. The reaction is too slow to affect the kinetic results described below.

Typical data are plotted in Figure 8 which shows the least-squares plots of $\ln(A_0 - A_\infty/A - A_\infty)$ vs. time (min) for various constant CO pressures. The slopes of these lines are the pseudo-first-order rate constants, k_{obsd}. The average values obtained for k_{obsd} ($s^{-1} \times 10^4$) at the indicated CO pressure are as follows: k (P_{CO} atm) 0.75 (0.04), 1.53 (0.10), 2.13 (0.20), 2.42 (0.30), 3.33 (1.00). It is seen that increasing the CO pressure increases the rate, but the rates approach a limiting value.

Figure 9 is a plot of $1/k_{obsd}$ vs. $1/P_{CO}$. The straight line (r = 0.9991) has a slope of 427 ± 25 s-atm and an intercept of 2540 ± 280 s at $1/P_{CO}$ = 0.0 (all errors are at the 95% confidence levels).

At P_{CO} = 1.0 atm, the rate is already very close to the limiting rate which corresponds to $1/P_{CO}$ = 0.0 on the graph in Figure 9. Therefore, the rates of the reaction at P_{CO} = 1.0 atm vs. temperature allows one to calculate the activation energy of the CO-independent rate constant. The observed, pseudo-first-order rate constants at 0.0, 6.0, 13.0, and 27.0 °C were 1.20, 1.35, 1.80, and 3.33 × 10^{-4} s^{-1}, respectively. Figure 10 is a plot of the reciprocal of these rates vs. $1/T$. The activation energy calculated from the slope is 6 ± 2 kcal/mol (95% confidence level).

The μ-fluorenylidene complex **2c** showed no reaction with CO even at 49 atm and 55 °C after 12 h.

In one experiment, a toluene solution of **2a** was allowed to react with 3 equiv of ^{13}CO (99% ^{13}C) in a closed system connected to a gas burette. The Ph_2CCO formed was collected on a cold finger and dissolved in toluene. A GC–MS determination of the ^{13}C-enrichment in Ph_2CHCO_2H, the hydrolysis product of the ketene, gave a ratio (F) of $*C/(*C + C)$ = 0.39 ± 0.05 for the parent ion (av of six scans).

With C_2H_4. At 50 °C and under a pressure of 3 atm of C_2H_4, **2a** reacted slowly to give $Cp_2Mo_2(CO)_6$ as the only product which could be identified in the ^1H NMR spectrum of the reaction mixture. A GC–MS of the high boiling organic products (collected on a cold finger under vacuum) indicated the presence of

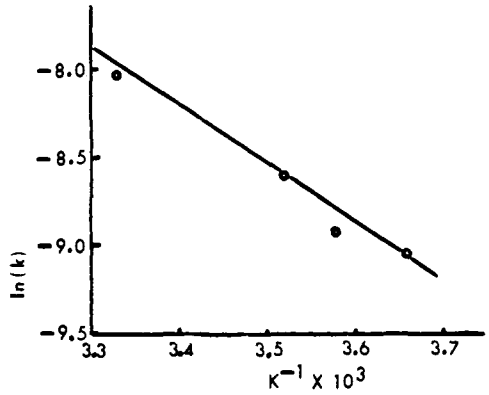

Figure 10. Arrhenius plot of $\ln(k_{obsd})$ vs. 1/temp (K) for the reaction of $Cp_2Mo_2(CO)_4(\mu,\eta^3\text{-}CPh_2)$, **2a**, with CO (P = 1 atm.).

$Ph_2CH—CH=CH_2$ or $Ph_2C=CH—Me$ by a computer match of the mass spectrum with library spectra. In addition, Ph_2CH_2 from the thermal decomposition of **2a** was also detected. The μ-fluorenylidene **2c** failed to react with C_2H_4 after 12 h at 50 °C under 53 atm of C_2H_4.

With RC≡CR. The reaction of **2a′**, $Cp'_2Mo(CO)_4(\mu\text{-}CPh_2)$, with 2-butyne at 25 °C gave a 75% isolated yield of the alkyne adduct $Cp'_2Mo_2(CO)_4(\mu\text{-}\eta^2\text{-}MeCCMe)$ (**11**) and trace amounts of Ph_2CH_2 and Ph_2CO. The major organic product was determined to be 1,1-diphenyl-2,3-dimethylcyclopropene by GC–MS analysis (eq 7).

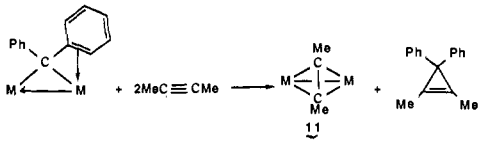

(7)

11

The reaction of **2a′** with PhC≡CPh also gave the alkyne adduct $M_2(\mu\text{-}\eta^2\text{-}PhCCPh)$, trace amounts of Ph_2CH_2 and Ph_2CCO, and about 15 other products. No evidence was found for the formation of tetraphenylcyclopropene.

In contrast, the μ-fluorenylidene complex **2c** did not react with RCCR (R = Et, Ph, Me_3Si) even at 80 °C after 4 h.

With Phosphines. The reactions of **2a** with alkyl phosphines are exceedingly complex. ^{31}P NMR spectra of the reaction mixtures indicated the presence of many compounds including signals in the region expected for ylides, e.g., $R_3P{=}CPh_2$. The only organometallic product isolated from the reaction with Me_3P was $[CpMo(CO)_2(PMe_3)_2]^+[CpMo(CO)_3]^-$ (**12**). The identity of the compound was established unequivocally by a single-crystal X-ray structure determination.[39]

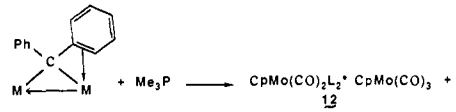

(8)

12

EHMO Analysis

It is apparent from the preceding results that the μ-diarylmethylene complexes **2a** and **2b** are much more reactive toward small molecules than is the μ-fluorenylidene complex **2c**. We thought this result was rather surprising since **2c** contains a formal Mo=Mo double bond and is therefore coordinatively unsaturated. The coordinative unsaturation in the triply bonded molecule **1** imparts a high reactivity to the molecule as compared to its saturated analogue $Cp_2Mo_2(CO)_6$. The following question arose: why doesn't the unsaturation present in **2c** impart the enhanced electrophilic character expected for such unsaturation?

A series of EHMO calculations (see Appendix) was performed to see if there were any electronic effects responsible for the difference in chemical behavior between **2a** and **2c**. The calculations were performed for a model compound in which the

(39) Our structural parameters are very similar to those recently reported: Schubert, U.; Ackermann, K.; Janta, R.; Voran, S.; Malisch, W. *Chem. Ber.* **1982**, *115*, 2003.

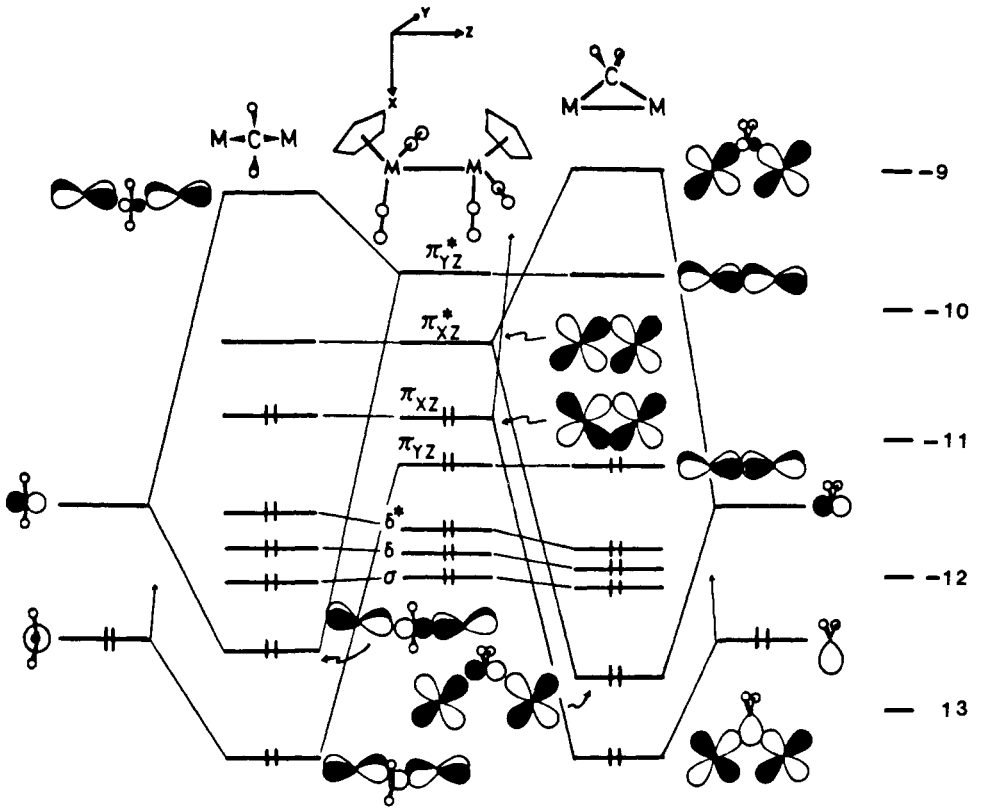

Figure 11. EHMO energy level diagram for the interaction of a CH_2 fragment with the $Cp_2Mo_2(CO)_4$ fragment with the atomic coordinates of the latter idealized from the structure of **2c**. The levels on the right correspond to model **2cM** and those on the left to **2aM** (see text).

bridging alkylidene groups of **2a** and **2c** were replaced with a μ-CH_2 group. These model μ-methylene complexes will be denoted by **2aM** and **2cM**.

In the first instance, a much simplified interaction scheme between the M_2 fragment and the μ-CH_2 group was calculated in order to isolate the salient electronic features. The energy levels and interacting orbitals are shown in Figure 11. In the central column, the energy levels corresponding to an isolated M_2 fragment having the same atomic coordinates as found experimentally for **2c** are shown. As expected, there is a formal M≡M triple bond with the electron configuration $\sigma^2\delta^2\delta^{*2}\pi^2_{xy}\pi^2_{xz}$. However, an orbital population analysis shows that only two orbitals make a substantial contribution to M–M bonding: the overlap population (POP) of the π_{xz} is 0.228 and accounts for 50% of the total M–M POP, and the POP of the σ orbital is 0.150 or 33% of the total. The low symmetry of the molecule allows mixing of the π_{yz} with orbital components having δ^* and π^* symmetry so that the POP of the "π_{yz}" orbital is only 0.034. Therefore, although a formal M≡M triple bond exists in the isolated M_2 fragment, the orbital population analysis suggests that an M=M double bond formulation is more appropriate.

In **2c**, the μ-alkylidene carbon lies nearly in the xz plane of Figure 11. When this interaction is modeled in **2cM** by placing the μ-CH_2 group on the $-x$ axis, the energy levels and orbitals diagrammed in the right hand column of Figure 11 result. The sp hybrid of the CH_2 fragment finds a good symmetry and energy match with the π_{xz} orbital of the M_2 fragment and forms the bonding MO shown in Figure 11 (the corresponding antibonding orbital lies at high energy and is not shown in the figure). The vacant p orbital of the μ-CH_2 group finds its symmetry match with the π^*_{xz} orbital and forms the bonding and antibonding MOs as shown. The σ, δ, and π^* orbitals of the M_2 fragment are essentially unperturbed, and the π_{yz} orbital is nonbonding with respect to the μ-CH_2 fragment.

The interactions described above convert the metal–metal π_{xz} and π^*_{xz} orbitals into two M–C bonding orbitals corresponding to the two M–C bonds. The total M–M POP falls from 0.461 in the M_2 fragment to 0.21 in the μ-methylene **2cM**. Nearly all this decrease results from shifting the electron density in the M–M π_{xz} orbital to M–C bonding (the total POP for an M–C bond in **2cM** is 0.50).

Note that the bonding of the CH_2 fragment to the M_2 fragment lowers the *formal* bond order from 3 to 2 as expected from electron-counting arguments and the structural parameters found for **2c**. However, the population analysis shows that the σ-bond in **2cM** accounts for 71% of the total M–M POP, i.e., the population analysis suggests that there is only an M–M single bond present. These differences between the formal bond orders and the bond orders assigned on the basis of population analyses emphasize the uncertainties associated with assigning bond orders in low-symmetry complexes, especially when a bridging group is present.

As Figure 3 shows, the μ-alkylidene carbon in **2a** lies in the yz-plane of Figure 11 or at essentially right angles to the placement in **2c**. The bonding in **2a** was first modelled by placing the μ-CH_2 fragment on the $-y$ axis, leaving the carbonyl groups in the same positions as found for **2c**. Now the sp hybrid and p orbitals of the μ-CH_2 group find their symmetry matches with the π_{yz} and π^*_{yz} orbitals of the M_2 fragment (left side of Figure 11), but otherwise the bonding picture remains much the same as described above for **2cM**. The most striking difference between the energy levels of **2aM** and **2cM** is the small HOMO–LUMO gap (0.45 eV) for the former as compared to the latter (1.30 eV). In **2aM**, the LUMO is a good acceptor orbital and provides a low-energy-frontier orbital for nucleophilic attack by a small molecule. The relatively high energy LUMO of **2cM** is not a good acceptor orbital.

Insofar as these simplified models represent the bonding in **2a** and **2c**, we have an explanation of the fact that **2c** is much less reactive toward small nucleophiles than is **2a**. However, we have not yet modeled the interaction of the phenyl group with the metal that is present in **2a**. The calculated energies of the MOs for **2aM** with the carbonyls distorted to the positions as found in the structure of **2a** reinforce the qualitative aspects of the conclusions reached above. The lower symmetry causes extensive mixing of the orbitals (Figure 12—Supplementary Material), but the calculated HOMO–LUMO gap remains small (0.45 eV). However, the LUMO is now localized on Mo1 (53% on Mo1, 3% on Mo2).

This LUMO is a d-p hybrid (diagrammed below) which points out to one side of the μ-CH_2 group. It is this acceptor orbital which the phenyl group in **2a** utilizes for bonding to form the π-benzylic structure.

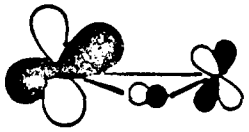

The total energy of **2cM** was calculated to be 42 kcal/mol lower than the total energy of **2aM**, i.e., for a μ-CH_2 group, the structure corresponding to that found for the μ-fluorenylidene **2c** is the intrinsically more stable one. We believe that unfavorable steric interactions between the μ-diphenylmethylene and the Cp groups forces the μ-CPh_2 ligand to one side. The concommitant distortion of the CO ligands produces the low-energy-acceptor orbital diagrammed above, and one phenyl ring then bonds to the metal by donating ring π-electrons into the acceptor orbital. This bonding interaction then stabilizes the observed, π-benzylic structure. Unfortunately, the EHMO method is not suited for modeling these energy changes.

It is proposed (see Discussion) that the high reactivity of **2a** or **2b** results as a consequence of the aryl ring detaching from the metal to give an intermediate with a low-energy-acceptor orbital. Since the aryl groups are tied together to form a planar structure in the μ-fluorenylidene complex, no appreciable steric forces exist between the Cp groups and the μ-fluorenylidene fragment. Complex **2c** then adopts the intrinsically stable structure calculated for **2cM**. This structure does not have a low-energy acceptor orbital, and the reactivity of **2c** toward small nucleophiles is diminished.

Discussion of Reactivity

The salient features of the solid state and solution structures of the μ-alkylidenes and some of their reaction products were discussed in the preceeding sections. This discussion will attempt to develop a comprehensive picture of the reactivity of the μ-alkylidenes **2a** and **2c** and show how the structural features, kinetics, and EHMO results can be fitted together to form an integrated picture.

Kinetics of the Reaction of 2a with CO. The kinetic behavior described above is characteristic of reactions in which there is a preequilibrium step. In the case at hand, the kinetics are consistent with the model shown in eq 9-11.

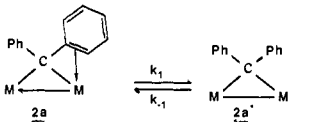

(9)

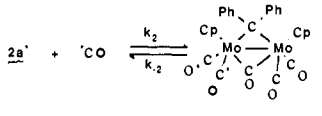

(10)

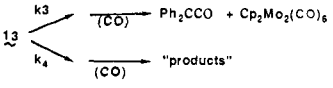

(11)

In the range of CO pressures investigated, k_3 and k_4 may be lumped into one effective rate constant, k', for the rate of transformation of **13** into products. Then the steady-state approximation leads to the rate expression

$$\text{rate} = \frac{k_1 k_2 k'[\mathbf{2a}][\text{CO}]}{k_{-1}(k_{-2} + k') + k_2 k'[\text{CO}]} \quad (12)$$

$$\text{rate} = k_{\text{obsd}}[\mathbf{2a}] \quad (13)$$

$$\frac{1}{k_{\text{obsd}}} = \frac{1}{k_1} + \frac{k_{-1}(k_{-2} + k')}{k_1 k_2 k'[\text{CO}]} \quad (14)$$

Thus, a plot (Figure 9) of the reciprocal of the observed first-order rate constant, $1/k_{\text{obsd}}$, vs. the reciprocal of the CO pressure yields a straight line with intercept $1/k_1$ and slope = $k_{-1}(k_{-2} + k')/k_1 k_2 k'$. From the observed intercept and slope, the values $k_1 = 3.9 \pm 0.3 \times 10^{-4}$ s^{-1} and $k_2 k'/k_{-1}(k_{-2} + k') = 6.0 \pm 0.6$ atm are obtained. Since $k_{\text{obsd}} \approx k_1$ at $P_{\text{CO}} = 1$ atm, the slope of the line in Figure 10 gives the activation energy, $E_a = 6 \pm 2$ kcal/mol, for the process which generates an open coordination site for attack by CO. This process is presumably the detachment of the phenyl group (eq 9) that generates the low-energy-acceptor orbital revealed by the EHMO calculations. Mechanisms which require free Ph_2C are precluded by previous crossover experiments which show that free diphenylmethylene is not formed under the reaction conditions.[21]

It is interesting to compare the activation energy (6 ± 2 kcal/mol) found for the preequilibrium step, eq 9, with the E_a for the fluxional process which averages the environments of the Cp and Ar groups in compounds **2**. The latter was estimated to be ca. 10 ± 2 kcal/mol from the coalescence temperatures of the various peaks. The former E_a, associated with the opening of a vacant coordination site by detachment of the phenyl coordinated to Mo, might be expected to be similar to the E_a for the fluxional process which must also involve disruption of the Mo-Ph coordination. In fact, the two values are of similar magnitude. The slightly lower value found for the CO addition reactions suggests that a smaller rearrangement of the coordination sphere is required to generate a vacant site than to cause the equivalencing of the two halves of the molecule.

The course of the reaction is much more complex than the clean kinetics would suggest. The products obtained depend on the CO pressure. Therefore, there must be a "branch point" later in the mechanism than the kinetically important reactions. This branch point is represented by eq 11. At higher CO pressures (4 atm) and higher temperatures (55 °C), $Ph_2C{=}C{=}O$ and $Cp_2Mo_2(CO)_6$ are the major products. At lower P_{CO} and lower temperatures, a second organometallic product is formed, and very little $Ph_2C{=}C{=}O$ is detected in the IR spectra. Unfortunately, our attempts to identify either the organic product(s) or the new organometallic species were unsuccessful.

In light of the complexity of the reaction and the fact that Ph_2CCO is a minor product at $P_{\text{CO}} = 1$ atm, the results of the ^{13}CO labeling experiment are difficult to interpret. The observed enrichment factor, $F = {}^*C/({}^*C + C) = 0.39 \pm 0.05$ is close to the value $3/(3 + 4) = 0.43$ which would indicate complete scrambling of the CO pool (3 added *CO + 4CO in **2a**) before Ph_2CCO formation occurs. An alternate interpretation could be that the Ph_2CCO is formed by more than one pathway. Each pathway could have a different rate of incorporation of *CO, and the observed enrichment factor would then be the weighted average for each path. The simplest case might involve two paths. Path A incorporates 100% *CO in the product and accounts for 39% of the product formed. Path B incorporates no *CO and accounts for the balance of the product.

Formation of ketene-derived products from the reaction of alkylidene complexes and CO has been observed previously. Geoffroy et al. have studied the reactions of triosmium clusters which contain a μ-CH_2 function with CO.[40] The products are μ-(CC) ketene clusters. Labeling studies showed that the exogenous *CO was not incorporated in the ketene ligand. The reactions of $[Cp(CO)_2Ru]_2(\mu\text{-}CH_2)$ suggest that CO insertion occurs in a two-step mechanism.[17a] The first step is intramolecular CO insertion to form $Cp(CO)Ru(\mu\text{-}\eta^2\text{-}CH_2CO)Ru(CO)_2Cp$, followed by the second step, addition of CO to the coordinatively unsaturated Ru. Ketene formation has also been observed in the reactions of mononuclear alkylidenes.[41,42]

Attempts To Trap Intermediate 13. Since the kinetic data were readily interpreted by the mechanistic scheme represented in eq 9-11, we attempted to trap the proposed intermediate **13** by adding

(40) (a) Morrison, E. D.; Steinmetz, G. R.; Geoffroy, G. L.; Fultz, W. C.; Rheingold, A. L. *J. Am. Chem. Soc.* **1984**, *106*, 4783. (b) Morrison, E. D.; Geoffroy, G. L. *Ibid.* **1985**, *107*, 3541.

(41) Herrmann, W. A.; Planck, J. *Angew. Chem., Int. Ed. Engl.* **1978**, *17*, 525.

(42) Fischer, H. *Angew. Chem.* **1983**, *95*, 913.

nucleophiles other than CO. Trimethylphosphine reacted rapidly with **2a**, but the product mixture was extremely complex. The NMR spectra of the reaction mixtures indicated the presence of many compounds, including phosphorus ylides. The only organometallic product isolated was the salt $[CpMo(CO)_2L_2][CpMo(CO)_3]$ (**12**, L = Me_3P) (eq 8).

Isonitriles also gave an exceedingly complex mixture when allowed to react with **2a**. However, the reaction of *i*-PrNC with the less reactive fluorenylidene complex **2c** gave the keteneimine adduct **7** (eq 4) as the major product of the reaction. Adduct **7** is related to the structurally characterized **8** only in having a terminal CO replaced by a terminal isonitrile.

Adducts **7** and **8** are imine derivatives of ketene complexes and may serve as models for the latter. Thus, structure **14** may be

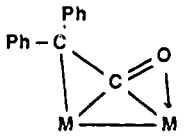

14

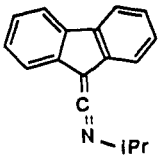

15

the penultimate product in the latter stages of the mechanistic pathway when **2a** reacts with CO to give $Ph_2C{=}CO$ and $Cp_2Mo_2(CO)_6$ (cf. eq 11). It is interesting to note that neither $Ph_2C{=}CO$ nor **15** react with **1** to give adducts. Once the ketene is ejected from the dimetal fragmental, steric barriers prevent recoordination.

Reactions with C_2H_4 and Alkynes. Since **2a** reacts with C_2H_4 and alkynes and **2c** does not, and since **2a** can rearrange to **2a*** which has a low-lying-acceptor orbital whereas **2c** cannot, we assume that the intermediate **2a*** (eq 9) plays an important role in the reactions of **2a** with C_2H_4 and alkynes.

With C_2H_4, the organic product appears (GC–MS) to be $Ph_2CH{-}CH{=}CH_2$ (or its tautomer, $Ph_2C{=}CH{-}CH_3$) formed by insertion of Ph_2C into the C–H bond of the olefin. A possible mechanism for this reaction is shown in eq 15. However, the

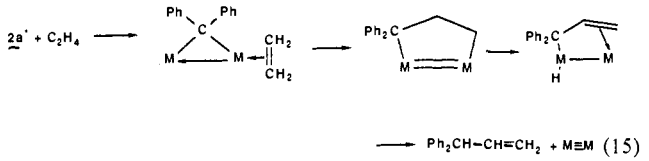

(15)

reaction is not very clean, and $Cp_2Mo_2(CO)_6$, formed from **1** and CO released during the reaction by other decomposition paths, is a major product. This mechanism is very similar to some proposed by Summer et al.[43] and by Rudler et al.[3]

The reaction of **2a** with 2-butyne cleanly affords the alkyne adduct **11** and 1,1-diphenyl-2,3-dimethylcyclopropene (eq 7). A proposed mechanism is shown in eq 16 and 17.

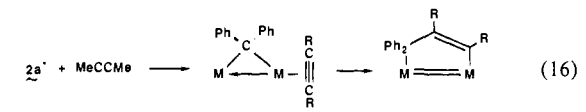

(16)

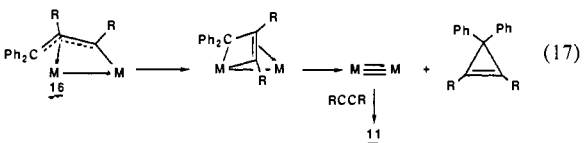

(17)

Complexes similar to **16** have been isolated from the reactions of μ-alkylidenes with alkynes in several instances.[43-48] Green et al. have observed the reverse of eq 17 in the ring-opening reaction of **1** and 1,1-dimethylcyclopropene (eq 18).[26]

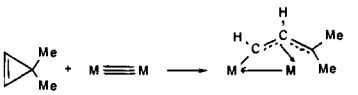

(18)

With Ar_2CN_2 (Ar = *p*-tolyl). The reaction of **2b** with Ar_2CN_2 to give **6** (eq 3) can be interpreted as proceeding through an intermediate similar to **13** (eq 10). Initial detachment of the phenyl ring (eq 9) is now followed by the nucleophilic attack of the diazoalkane (eq 19). Symmetric bridge opening converts **19** to **20**, and an "internal" displacement of CO by the lone pair on nitrogen leads to the final product **6** (eq 20).

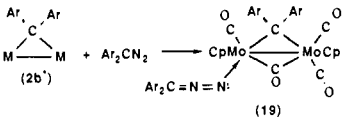

(19)

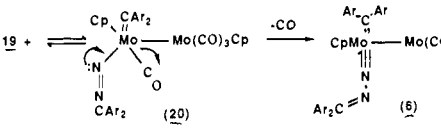

(20)

Reaction of 2a with H_2. The results of the reaction of **2a** with an H_2/D_2 mixture suggests that the primary reaction pathway may be represented by the sequence of events depicted in eq 21.

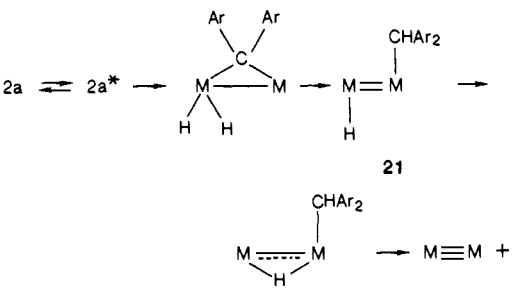

(21)

Detachment of one phenyl group gives the coordinatively unsaturated intermediate **2a***, which reacts with H_2 and ultimately expels Ar_2CH_2 from M_2 fragment by reductive elimination.

Conclusions. The μ-diarylmethylene complexes **2a** and **2b** undergo many of the types of reactions postulated for μ-CH_2 groups on the surfaces of solid catalysts in the catalyzed hydrogenation of CO.[5-7] These include hydrogenation and coupling with CO, alkenes, and alkynes. Bridge → terminal conversion for the alkylidene fragment was observed in one reaction. Bridge → terminal → bridge' transformations are thought to be responsible for CH_2 mobility on metal surfaces. EHMO calculations provide a rationale for the difference between the ground-state structures of **2a** and **2c** as well as an explanation for the enhanced reactivity of the former vis-a-vis the latter.

Experimental Section

Experimental. All experimental work involving air-sensitive material was carried out under pure N_2 in an inert atmosphere box equipped with a purification train or in standard Schlenk ware. Toluene, benzene, ether, and THF were dried over sodium benzophenone and distilled under N_2 immediately prior to use. Methylene chloride was dried over P_4O_{10}. IR spectra were recorded on PE 457 or 1330 instruments, NMR spectra were recorded on a Bruker WM-360 spectrometer (360 MHz for ^1H, 90.5 MHz for ^{13}C, and 55.25 MHz for ^2D). Unless otherwise noted, the ambient temperature for NMR spectra was ca. 28 °C. GC–MS samples were analyzed on a Finnigan 4023 quadrupole analyzer instrument equipped with computerized data handling capabilities. Elemental analyses were performed by Galbraith Laboratories, Knoxville, TN. The

(43) Summer, C. E., Jr.; Collier, J. A.; Pettit, R. *Organometallics* **1982**, *1*, 1350.
(44) Dyke, A. F.; Knox, S. A. R.; Naish, P. J.; Taylor, G. E. *J. Chem. Soc., Chem. Commun.* **1980**, 803.
(45) Dickson, R. S.; Fallon, G. D.; Nesbit, R. J.; Pain, G. N. *Organometallics* **1985**, *4*, 355.
(46) Müller, J.; Passon, B.; Pickardt, J. *J. Organomet. Chem.* **1982**, *236*, C11.
(47) Clauss, A. D.; Shapley, J. R.; Wilson, S. R. *J. Am. Chem. Soc.* **1981**, *103*, 7387.
(48) Casey, C. P.; Miles, W. H.; Fagan, P. J.; Haller, K. J. *Organometallics* **1985**, *4*, 559.

Table IV. Crystal and Data Statistics

	$Cp_2Mo_2(CO)_4(CAr_2)$·PhMe (**2b**)	$Cp_2'Mo_2(CO)_4(\mu\text{-}CAr_2')$ (**2c**)	$Cp_2'Mo_2(CO)_4(i\text{-}PrNCC_{13}H_8)$ (**8**)
color	dark red	red-black	black
chem. formula	$C_{36}H_{32}Mo_2O_4$	$C_{29}H_{22}Mo_2O_4$	$C_{33}H_{29}Mo_2NO_4$
mol wt	720.2	626.2	695.2
a, b, c (Å)	18.481 (8), 19.095 (5), 10.065 (3)	11.716 (5), 12.152 (6), 17.488 (4)	8.486 (3), 20.16 (1), 16.75 (7)
α, β, γ (deg)	90.01 (2), 105.76 (3), 117.01 (3)	90.0, 108.77 (3), 90.0	90.0, 92.31 (7), 90.0
Z, ρ (g/mL), V (Å^3)	4, 1.55 (calcd), 3014 (2)	4, 1.76 (calcd), 2358 (2)	4, 1.71 (calcd), 2863 (4)
crystal dimen (mm)	0.15 × 0.22 × 0.23	0.28 × 0.21 × 0.11	0.11 × 0.08 × 0.30
space group	$P\bar{1}$	$P2_1/c$	$P2_1/c$
radiation	Mo Kα monochrom from graphite cryst	Mo Kα monochrom from graphite cryst	Mo Kα monochrom from graphite cryst
take off angle	4°	4°	4°
μ(Mo Kα, cm^{-1}) (abs corr)	8.50 (yes)	7.4 (no)	8.65 (no)
scan speed (deg/min)	2–12 variable	2–12 variable	2–15 variable
scan range	Mo Kα_1 −0.8° to Mo Kα_2 +0.8°	Mo Kα_1 −0.8° to Mo Kα_2 +0.8°	Mo Kα_1 −0.8° to Mo Kα_2 +0.8°
background/scan time	0.8	0.8	0.8
std reflcns	(0,2,1), (1,0,1), (3,$\bar{2}$,0)	(4,1,0), (2,3,$\bar{1}$), (1,1,7)	(2,0,0), (1,3,1), (2,3,2)
2θ limit	50°	50°	45°
reflcns	10 653 (6085 with $I > 3\sigma(I)$)	4905 (3381 with $I > 3\sigma(I)$)	3032 (2297 with $I > 3\sigma(I)$)
N_o/N_v	12.0	10.7	6.4
goodness of fit	2.40	1.40	2.91
R_1, R_2	0.057, 0.078	0.036, 0.056	0.045, 0.039

Table V. Atomic Coordinates for **2b·PhMe**

atom	x	y	z	atom	x	y	z
Mo1	0.3665 (1)	0.0607 (1)	0.0397 (1)	C25	0.1526 (8)	−0.0995 (7)	−0.2967 (12)
Mo2	0.3197 (1)	0.0023 (1)	0.3055 (1)	C26	0.2012 (7)	−0.1181 (7)	−0.1885 (12)
Mo3	0.3666 (1)	0.5607 (1)	0.3269 (1)	C27	0.2336 (7)	−0.0768 (7)	−0.0498 (11)
Mo4	0.3198 (1)	0.5023 (1)	0.0143 (1)	C28	0.1114 (9)	−0.1474 (8)	−0.4423 (14)
C1	0.4457 (9)	0.0583 (8)	0.2166 (14)	C5′	0.4897 (8)	0.6700 (8)	0.4552 (13)
O1	0.5119 (6)	0.0715 (6)	0.2910 (10)	C6′	0.4456 (9)	0.6308 (8)	0.5521 (14)
C2	0.3885 (8)	−0.0246 (8)	−0.0164 (14)	C7′	0.3679 (9)	0.6344 (8)	0.5141 (14)
O2	0.4060 (7)	−0.0719 (6)	−0.0459 (13)	C8′	0.3635 (8)	0.6765 (7)	0.4015 (13)
C3	0.3475 (8)	−0.0820 (7)	0.2791 (13)	C9′	0.4388 (8)	0.6979 (8)	0.3615 (13)
O3	0.3618 (6)	−0.1339 (6)	0.2688 (10)	C10′	0.2877 (9)	0.5476 (9)	−0.1971 (15)
C4	0.2082 (8)	−0.0898 (7)	0.2407 (12)	C11′	0.3295 (10)	0.5041 (9)	−0.2111 (15)
O4	0.1423 (6)	−0.1438 (6)	0.2055 (10)	C12′	0.4120 (10)	0.5417 (9)	−0.1238 (15)
C1′	0.4457 (9)	0.5584 (8)	0.2284 (13)	C13′	0.4233 (9)	0.6134 (9)	−0.0596 (14)
O1′	0.5118 (6)	0.5712 (6)	0.2205 (10)	C14′	0.3459 (9)	0.6157 (8)	−0.1043 (14)
C2′	0.3881 (8)	0.4748 (7)	0.4038 (14)	C15′	0.2108 (6)	0.5787 (6)	0.0711 (10)
O2′	0.4056 (6)	0.4282 (6)	0.4515 (12)	C16′	0.1259 (7)	0.5357 (7)	−0.0061 (12)
C3′	0.2082 (8)	0.4102 (8)	−0.0327 (12)	C17′	0.0770 (7)	0.5730 (7)	−0.0667 (12)
O3′	0.1418 (6)	0.3557 (6)	−0.0637 (10)	C18′	0.1135 (8)	0.6560 (7)	−0.0499 (12)
C4′	0.3479 (8)	0.4181 (7)	0.0686 (13)	C19′	0.1990 (8)	0.6997 (7)	0.0215 (12)
O4′	0.3616 (6)	0.3661 (6)	0.0930 (10)	C20′	0.2487 (7)	0.6631 (7)	0.0831 (11)
CB	0.2554 (6)	0.0337 (6)	0.1148 (10)	C21′	0.0570 (9)	0.6945 (9)	−0.1142 (14)
CB′	0.2554 (6)	0.5336 (6)	0.1409 (10)	C22′	0.2177 (7)	0.4882 (6)	0.2398 (11)
C5	0.3684 (9)	0.1349 (8)	−0.1472 (14)	C23′	0.2341 (7)	0.4233 (7)	0.2833 (11)
C6	0.4465 (8)	0.1306 (8)	−0.1059 (13)	C24′	0.2013 (7)	0.3817 (7)	0.3900 (12)
C7	0.4899 (8)	0.1702 (8)	0.0343 (13)	C25′	0.1533 (8)	0.4009 (8)	0.4492 (13)
C8	0.4388 (8)	0.1983 (7)	0.0768 (13)	C26′	0.1387 (8)	0.4668 (7)	0.4086 (12)
C9	0.3645 (8)	0.1769 (7)	−0.0367 (13)	C27′	0.1703 (7)	0.5091 (7)	0.3096 (11)
C10	0.3466 (9)	0.1165 (8)	0.4504 (14)	C28′	0.1119 (9)	0.3527 (8)	0.5533 (14)
C11	0.4240 (9)	0.1135 (9)	0.4826 (15)	CT1	0.1755 (11)	0.1665 (10)	−0.4593 (17)
C12	0.4126 (10)	0.0421 (9)	0.5368 (15)	CT2	0.2569 (20)	0.2344 (19)	−0.3848 (32)
C13	0.3282 (10)	0.0036 (9)	0.5392 (15)	CT3	0.2782 (16)	0.2714 (15)	−0.2769 (27)
C14	0.2872 (9)	0.0468 (9)	0.4847 (14)	CT4	0.1983 (11)	0.2327 (10)	−0.2167 (16)
C15	0.2108 (7)	0.0788 (6)	0.1402 (10)	CT5	0.0578 (18)	0.1394 (16)	−0.2376 (27)
C16	0.2488 (7)	0.1628 (7)	0.1664 (11)	CT6	0.1219 (15)	0.1711 (13)	−0.2752 (22)
C17	0.1987 (8)	0.1996 (7)	0.1765 (12)	CT7	0.1021 (13)	0.1276 (12)	−0.4266 (21)
C18	0.1135 (8)	0.1555 (7)	0.1638 (12)	CT1′	0.8769 (15)	0.3272 (13)	0.6025 (22)
C19	0.0772 (8)	0.0726 (7)	0.1439 (12)	CT2′	0.8984 (14)	0.3729 (13)	0.4705 (21)
C20	0.1257 (7)	0.0354 (7)	0.1320 (11)	CT3′	0.8231 (12)	0.3317 (11)	0.3637 (18)
C21	0.0574 (9)	0.1947 (9)	0.1708 (15)	CT4′	0.7430 (19)	0.2650 (18)	0.3602 (29)
C22	0.2176 (7)	−0.0122 (6)	−0.0216 (11)	CT5′	0.7232 (16)	0.2283 (16)	0.4483 (27)
C23	0.1706 (7)	0.0094 (7)	−0.1397 (11)	CT6′	0.8012 (11)	0.2674 (10)	0.5861 (16)
C24	0.1384 (8)	−0.0337 (7)	−0.2688 (12)	CT7′	0.9399 (18)	0.3586 (16)	0.7043 (27)

synthesis of the μ-alkylidene complexes **2a–c** was reported elsewhere.[21]

Reaction of $(C_5H_4CH_3)_2Mo_2(CO)_4(\mu\text{-}C_{13}H_8)$, 2c, and Hydrogen. A solution of 0.08 mmol (0.05 g) of $(C_5H_4CH_3)_2Mo_2(CO)_4(\mu\text{-}C_{13}H_8)$, **2c**, was dissolved in 10 mL of toluene and placed in a 50-mL stainless steel bomb. This was pressurized to 750 psi of H_2 and warmed to 50 °C for 12 h. The toluene was concentrated in vacuo to dryness. An IR spectrum of the residue showed it to be primarily $(C_5H_4CH_3)_2Mo_2(CO)_4$ (KBr, cm^{-1}): ν_{CO}, 1950, 1875. The residue was sublimed at 80 °C, 0.5 mmHg vacuum for 1 h. A white solid was obtained, the ^{1}H NMR (C_6D_6, 83.80 (s, CH_2), 7.68 (d), 744 (d), 7.27 (t), 7.20 (t), 7.14 (s) (Ar)) and IR (KBr, 730 cm^{-1}) of which showed it to be fluorene.

Attempted Reaction of $(C_5H_4CH_3)_2Mo_2(CO)_4(\mu\text{-}C_{13}H_8)$, 2c, with Carbon Monoxide and Ethylene. A solution of $(C_5H_4CH_3)_2Mo_2(CO)_4$-$(\mu\text{-}C_{13}H_8)$ in toluene was placed in a stainless steel bomb. This was pressurized to 700 psi with CO and warmed to 50 °C for 12 h. An IR spectrum (C_7H_8, ν_{CO}, 1980, 1925, 1850 cm^{-1}) of the reaction mixture

indicated that no reaction had occurred.

A solution of $(C_5H_4CH_3)_2Mo_2(CO)_4(\mu\text{-}C_{13}H_8)$ in toluene was placed in a stainless steel bomb. This was pressurized to 650 psi of C_2H_4 and warmed to 65 °C for 12 h. An IR spectrum of the reaction mixture (C_7H_8, ν_{CO}, 1982, 1930, 1845 cm^{-1}) indicated that no reaction had occurred.

Synthesis of $(C_5H_4CH_3)_2Mo_2(CO)_3(NCC_3H_7)(\mu\text{-}N(C_3H_7)C_{14}H_8)$, 7, from $(C_5H_4CH_3)_2Mo_2(\mu\text{-}C_{13}H_8)$ and Isopropyl Isocyanide. In a 100-mL Schlenk flask was dissolved 0.50 mmol (0.31 g) of $(C_5H_4CH_3)_2Mo_2(CO)_4(\mu\text{-}C_{13}H_8)$ in 15 mL of toluene. To this was added a solution of 1.0 mmol (0.09 mL) of isopropyl isocyanide in 10 mL of toluene via syringe over a 10-min period. The mixture was stirred at room temperature for 6 h, during which time the color of the solution turned from brick-red to orange, and gas evolution was observed. The toluene was concentrated under vacuum, hexane was added, and the mixture cooled to −23 °C overnight. An oily brown solid was filtered and discarded. The filtrate was concentrated under vacuum, hexane was added, and the mixture cooled to −23 °C overnight. A black, microcrystalline solid was filtered, washed with hexane, and dried: IR (KBr, cm^{-1}) $\nu_{C\equiv N}$ 2120, ν_{CO} 1895, 1805; ^1H NMR (360 MHz, C_6D_6, 30 °C) δ 0.67 (d, $CH(CH_3)_2$), 0.83 (d, $CH(CH_3)_2$), 0.96 (d, $CH(CH_3)_2$), 1.26 (d, $CH(CH_3)_2$), 1.73 (s, $C_5H_4CH_3$), 1.88 (s, $C_5H_4CH_3$), 3.77 (m, $CH(CH_3)_2$, 5.07 (m, $CH(CH_3)_2$), 4.56–5.23 (two overlapping ABCD patterns, $C_5H_4CH_3$), 7.27 (q, Ar), 7.29 (t, Ar), 7.39 (t, Ar), 7.41 (d, Ar), 7.49 (t, Ar), 7.53 (d, Ar); mp > 280 °C. Anal. Calcd for $C_{36}H_{36}N_2O_3Mo_2$: C, 58.7; H, 4.9; N, 3.8. Found: C, 58.9; H, 4.6; N, 4.5.

Attempted Reaction of $(C_5H_4CH_3)_2Mo_2(CO)_4(\mu\text{-}C_{13}H_8)$, 2c, and Various Acetylenes. No reaction was observed when toluene solutions of **2c** were heated to 80 °C for 4–5 h with equimolar amounts of 3-hexyne, diphenylacetylene, or bis(trimethylsilyl)acetylene.

Reaction of $Cp'_2Mo_2(CO)_4(\mu\text{-}CPh_2)$ and 2-Butyne. In a 100-mL Schlenk flask was dissolved 0.40 mmol (0.25 g) of $Cp_2'Mo_2(CO)_4(\mu\text{-}CPh_2)$ in 10 mL of benzene. To this was added a solution of 0.70 mmol (0.06 mL) of 2-butyne in 2 mL of benzene. The mixture was stirred at room temperature for 3 h. An IR spectrum of the mixture indicated that only $Cp'_2Mo_2(CO)_4(MeC\equiv CMe)$ was present (IR, C_6H_6, ν_{CO} 1980, 1960, 1903 cm^{-1}). The benzene was removed under vacuum, and a GC of the volatiles indicated that no organic products were present. The residue was sublimed at 90–100 °C, 0.5 mmHg vacuum for 2 h. A white solid was rinsed from the cold finger with toluene; the GC–MS of this solution indicated the presence of 0.003 mmol of Ph_2CH_2 and 0.007 mmol of Ph_2CCO (the response factors for these compounds were calculated from a standard solution, with dodecane as the internal standard). The primary organic product was found to be 1,2-dimethyl-3,3-diphenylcyclopropene: *m/e* 220, P^+ (calcd 220), 205 ($P^+ - CH_3$, base), 143 ($P^+ - Ph$), 77 (Ph^+).

Reaction of $Cp_2'Mo_2(CO)_4(\mu\text{-}CPh_2)$, 2a, and Diphenylacetylene. In a 100-mL Schlenk flask was dissolved 0.04 mmol (0.25 g) of $Cp_2'Mo_2(CO)_4(\mu\text{-}CPh_2)$ in 10 mL of benzene. To this was added a solution of 0.36 mmol (0.065 g) of diphenylacetylene in 5 mL of benzene, and the mixture was stirred at room temperature for 48 h. An IR spectrum of the reaction mixture (C_6H_6, ν_{CO} 1975, 1945, 1915, 1830 cm^{-1}) indicated the presence of $Cp_2'Mo_2(CO)_4(PhC\equiv CPh)$. The benzene was removed under vacuum, and a GC of the volatile fraction did not indicate that any organic products were present. The residue was sublimed at 80–90 °C, 0.5 mmHg vacuum for 2 h. A white solid was rinsed off the cold finger with toluene. A GC–MS study of this solution indicated the presence of trace quantities of Ph_2CH_2 and Ph_2CCO (<1% for each) together with ca. 15 other organic compounds which were not identified.

Kinetic Measurements of the Reaction of 2a with CO. Toluene solutions (10 mL, 1.43×10^{-2} M) of **2a** were placed in a 100-mL, 3-necked flask equipped with a gas inlet, a magnetic stirring bar, and a rubber septum for withdrawal of aliquots for IR spectra. Gas streams with varying proportions of CO and N_2 were prepared by mixing CO and N_2 in desired proportions with calibrated Matheson mass flow controllers. The total pressure of the mixtures was always 1.0 atm. The partial pressure of the CO is thus determined by the percent CO in the gas stream. These gas streams were admitted to the reaction vessel while the solutions of **2a** were vigorously stirred with a magnetic stirrer. Aliquots of the solution were periodically withdrawn by syringe through the septum for IR analysis. Typical data are shown in Figure 8. The temperature was held constant by either slush baths ($T < 25$ °C) or by an oil bath ($T > 25$ °C) whose temperature was controlled by an RFD Industries proportional temperature controller. The absorbances of the 1830 and 1780 cm^{-1} peaks of the starting material were measured as a function of time, and the rate constants obtained from the two sets of data were averaged.

In several instances, the reaction products were isolated by first concentrating the toluene solution and cooling the concentrate to 0 °C. Typically, 50–75% yields of crystalline $Cp_2Mo_2(CO)_6$ were obtained at this step. The solvent was removed from the filtrate from the first crop to give a red-brown oil containing a small amount of $Cp_2Mo_2(CO)_6$, a small amount of an organometallic which decomposed (mainly to $Cp_2Mo_2(CO)_6$) upon further purification attempts, and the volatile organic products. The latter were collected by short-path vacuum distillation to a cold finger condenser.

Table IX. Atomic Coordinates for **2c**

atom	*x*	*y*	*z*
Mo1	0.07072 (3)	0.22117 (3)	−0.13996 (2)
Mo2	0.05449 (3)	0.37656 (3)	−0.26110 (2)
C1	−0.0395 (4)	0.1318 (4)	−0.0679 (3)
C2	−0.0483 (4)	0.0668 (4)	−0.1363 (3)
C3	0.0665 (4)	0.0272 (4)	−0.1323 (3)
C4	0.1501 (4)	0.0690 (4)	−0.0595 (3)
C5	0.0858 (4)	0.1326 (4)	−0.0198 (3)
C6	−0.1404 (5)	0.1818 (5)	−0.0451 (3)
C7	0.0420 (4)	0.4025 (4)	−0.3969 (3)
C8	0.0867 (5)	0.5004 (4)	−0.3533 (3)
C9	−0.0040 (5)	0.5447 (4)	−0.3263 (3)
C11	−0.1047 (5)	0.4759 (4)	−0.3517 (3)
C10	−0.0759 (4)	0.3882 (4)	−0.3947 (3)
C12	0.1038 (5)	0.3325 (5)	−0.4428 (3)
C13	−0.0566 (3)	0.2332 (3)	−0.2607 (2)
C14	−0.0596 (4)	0.1412 (3)	−0.3167 (2)
C15	−0.1807 (3)	0.1083 (3)	−0.3576 (2)
C16	−0.2056 (4)	0.0234 (4)	−0.4142 (2)
C17	−0.1125 (4)	−0.0292 (4)	−0.4298 (3)
C18	0.0062 (4)	−0.0001 (4)	−0.3896 (3)
C19	0.0339 (4)	0.0849 (4)	−0.3338 (3)
C20	−0.1873 (3)	0.2516 (3)	−0.2718 (2)
C21	−0.2588 (3)	0.1766 (3)	−0.3284 (2)
C22	−0.3845 (4)	0.1759 (4)	−0.3478 (3)
C23	−0.4377 (4)	0.2496 (4)	−0.3111 (3)
C24	−0.3683 (4)	0.3249 (4)	−0.2547 (3)
C25	−0.2436 (4)	0.3263 (4)	−0.2353 (2)
C26	0.0214 (4)	0.3549 (3)	−0.0984 (2)
C27	0.2408 (4)	0.2741 (4)	−0.0898 (3)
C28	0.2038 (4)	0.2981 (4)	−0.2501 (3)
C29	0.1488 (4)	0.4775 (4)	−0.1715 (3)
O1	−0.0054 (3)	0.4240 (3)	−0.0624 (2)
O2	0.3385 (3)	0.2963 (3)	−0.0576 (2)
O3	0.2945 (3)	0.2640 (3)	−0.2529 (2)
O4	0.1968 (3)	0.5414 (3)	−0.1253 (2)

X-ray Structure Determinations. 1. $Cp_2Mo_2(CO)_4[\mu\text{-}C(C_6H_4\text{-}p\text{-}Me)_2]\cdot PhMe$ (2b·PhMe). All X-ray data were collected on a Syntex $P2_1$ diffractometer by using standard Syntex software. Cell parameters were determined from 15 accurately centered high angle reflections scattered in reciprocal space. Three standard reflections were measured every 50 reflections. Two sets of programs were used to solve the structures, an older package of programs, described previously,[49] and the newer SHELX package by G. Sheldrick. All computations were performed on an Amdahl 5860 computer. The weight factors used in the older (Oak Ridge) programs were $w = 4F_o^2/(\sigma^2(F_o^2) + (PF_o^2)^2)$ ($P = 0.04$). Relevant crystal and data collection statistics are in Table IV. The locations of the metal atoms were determined from a Patterson map, and the nonhydrogen atoms were located in subsequent difference maps.[49] The unit cell contains two independent molecules of **2b** and two independent molecules of toluene of solvation. The atoms of the latter are labeled CT*n* in the tables. Atoms labeled Mo1 and Mo2 are in one molecule, and Mo3 and Mo4 are in the other. The numbering scheme for the lighter atoms of the second molecule is identical with that shown for the first molecule in Figure 1 but are denoted in the tables by primed numbers.

The structure was refined with anisotropic temperature factors for the metals and for the atoms directly bonded to the metals. The remaining atoms were refined isotropically to cut down the computer time in the full matrix refinement. The final atomic positions are in Table V, and the temperature factors are in Table VI(S) (Supplementary Material). Table VII(S) contains a complete listing of bond distances and angles, and Table VIII(S) is the listing of F_o vs. F_c for **2b**·C_7H_8 ((S) denotes Supplementary Material).

2. $Cp_2Mo_2(CO)_4(\mu\text{-}CC_6H_8)$ (2c). Crystals of **2c** were grown from a toluene/hexane solution held at −20 °C. The metal atoms were located

(49) Sources of scattering factors, programs used in the structure solution and refinement, etc., have been described previously: Curtis, M. D.; Han, K. R. *Inorg. Chem.* **1985**, *24*, 378.

Table XIII. Fractional Atomic Coordinates for **8**

atom	x	y	z	U
Mo1	0.4144 (1)	−0.0798 (1)	0.2090 (1)	0.034
Mo2	0.3106 (1)	−0.1464 (1)	0.3630 (1)	0.033
C1	0.0585 (15)	−0.1818 (6)	0.3924 (8)	0.068
C2	0.0321 (11)	−0.1296 (7)	0.3408 (6)	0.054
C3	0.0896 (12)	−0.0718 (6)	0.3767 (6)	0.052
C4	0.1511 (12)	−0.0892 (6)	0.4535 (6)	0.055
C5	0.1357 (15)	−0.1568 (7)	0.4630 (7)	0.070
C6	0.2146 (16)	−0.0403 (7)	0.5159 (7)	0.096
C7	0.6724 (14)	−0.0407 (8)	0.1879 (8)	0.071
C8	0.6505 (16)	−0.0951 (7)	0.1377 (9)	0.077
C9	0.5279 (18)	−0.0836 (7)	0.0835 (7)	0.075
C10	0.4724 (16)	−0.0202 (7)	0.0975 (7)	0.072
C11	0.5677 (17)	0.0068 (6)	0.1606 (8)	0.067
C12	0.5562 (18)	0.0782 (6)	0.1910 (8)	0.100
C13	0.2584 (11)	−0.1618 (4)	0.1909 (5)	0.029
C14	0.1408 (11)	−0.1914 (4)	0.1513 (5)	0.032
C15	0.0655 (11)	−0.2568 (5)	0.1693 (5)	0.035
C16	−0.0550 (12)	−0.2700 (6)	0.1119 (6)	0.048
C17	−0.1350 (13)	−0.3279 (7)	0.1115 (7)	0.058
C18	−0.1035 (16)	−0.3715 (6)	0.1721 (9)	0.077
C19	0.0097 (14)	−0.3594 (5)	0.2318 (6)	0.059
C20	0.0968 (12)	−0.3017 (5)	0.2296 (6)	0.049
C21	0.0501 (13)	−0.1659 (5)	0.0805 (6)	0.043
C22	−0.0644 (12)	−0.2127 (6)	0.0571 (6)	0.046
C23	−0.1653 (14)	−0.2022 (7)	−0.0102 (7)	0.075
C24	−0.1455 (17)	−0.1432 (8)	−0.0527 (7)	0.080
C25	−0.0307 (17)	−0.0978 (6)	−0.0307 (7)	0.074
C26	0.0700 (15)	−0.1091 (6)	0.0359 (6)	0.065
C27	0.4739 (12)	−0.2415 (4)	0.2323 (5)	0.040
C28	0.4789 (13)	−0.2618 (5)	0.1439 (6)	0.055
C29	0.6410 (12)	−0.2325 (5)	0.2689 (6)	0.051
C30	0.2101 (16)	−0.0367 (5)	0.2032 (6)	0.053
C31	0.4285 (13)	−0.0321 (5)	0.3130 (6)	0.047
C32	0.3914 (13)	−0.2297 (6)	0.4040 (6)	0.050
C33	0.5012 (14)	−0.1251 (5)	0.4256 (6)	0.054
O30	0.0881 (10)	−0.0116 (4)	0.1962 (4)	0.067
O31	0.4460 (10)	0.0109 (4)	0.3591 (4)	0.067
O32	0.4349 (11)	−0.2800 (4)	0.4313 (5)	0.078
O33	0.6079 (10)	−0.1147 (4)	0.4667 (5)	0.086
N1	0.3726 (9)	−0.1822 (3)	0.2471 (4)	0.028

in a Patterson map, and all non-hydrogen atoms were found in the subsequent difference map. The structure was refined anisotropically. An absorption correction was not necessary. The numbering scheme is shown in Figure 3. Crystal and data collection statistics are in Table IV. Fractional coordinates are in Table IX, temperature factors are in Table X(S), a complete list of bond distances and angles are in Table XI(S), and Table XII(S) contains a listing of F_o vs. F_c ((S) denotes Supplementary Material).

$Cp_2Mo_2(CO)_4(\mu\text{-}\eta^1,\eta^2\text{-}i\text{-}PrNC{=}C_{13}H_8)$ (8). Crystals were grown from toluene/hexane at 0 °C. Data were reduced, and the structure was solved by using the SHELX package. Hydrogen atoms with fixed positions (C–H = 1.0 Å, U = 0.05) were included in the model. Table IV gives the relevant statistics. Final atomic positions are in Table XIII, temperature factors in Table XIV(S), complete listing of bond distances and angles in Table XV(S), and F_o vs. F_c in Table XVI(S) ((S) denotes Supplementary Material). The final weighting factor was $w = 1.372/(\sigma^2(F) + 0.0001F^2)$.

Acknowledgment. This work was supported by the National Science Foundation (Grants No. CHE-8206153 and CHE-8305235) and the Petroleum Research Fund administered by the American Chemical Society.

Appendix

The EHMO calculations were performed with Hoffmann's programs ICON8 and FMO with the weighted H_{ij} option.[50] The atomic parameters have been tabulated elsewhere.[51] The bond distances were idealized from those determined by X-ray diffraction, i.e., all C–C distances in the Cp ring were set at 1.43 Å, Mo–C(Cp) at 2.32 Å, C–H at 1.0 Å, C–O at 1.16 Å, and Mo–C(alkylidene) = 2.17 Å. Observed angles for **2c** were averaged so as to give strict C_2 symmetry to the model **2cM**. Actual angles obtained for the $Cp_2Mo_2(CO)_4$ fragment in **2a** were used for the calculations in **2aM**. The CH_2 unit was then placed onto this fragment symmetrically bridging the Mo–Mo bond with Mo–C = 2.17 Å.

Registry No. 2a, 107939-99-1; **2a′**, 107939-97-9; **2b**·PhMe, 107940-01-2; **2c′**, 85957-08-0; **7**, 107939-95-7; **8**, 107939-96-8; **11**, 107939-98-0; $(C_5H_4CH_3)_2Mo_2(CO)_4$, 69140-73-4; $Cp_2Mo_2(CO)_6$, 12091-64-4; CO, 124-38-9; C_2H_4, 74-85-1; CN-*i*-Pr, 598-45-8; $CH_3CH_2C{\equiv}CCH_2CH_3$, 928-49-4; $PhC{\equiv}CPh$, 501-65-5; $Me_3SiC{\equiv}CSiMe_3$, 14630-40-1; $CH_3C{\equiv}CCH_3$, 503-17-3; Ph_2CH_2, 101-81-5; Ph_2CO, 119-61-9; 1,3-dimethyl-3,3-diphenylcyclopropene, 42842-60-4; fluorene, 86-73-7.

Supplementary Material Available: Figure 12 (EHMO energy level diagram) and tables of thermal parameters, bond distances, and angles for **2b·PhMe**, **2c**, and **8** (15 pages); listings of F_o vs. F_c for **2b·PhMe**, **2c**, and **8** (49 pages). Ordering information is given on any current masthead page.

(50) Ammeter, J. H.; Burgi, H.-B.; Thibeault, J. C.; Hoffmann, R. *J. Am. Chem. Soc.* **1978**, *100*, 3686.
(51) Curtis, M. D.; Eisenstein, O. *Organometallics* **1984**, *3*, 887.